

Beyond maps: Patterns of formation processes at the Middle Pleistocene open-air site of Marathousa 1, Megalopolis Basin, Greece

D. Giusti^{a,*}, V. Tourloukis^a, G. E. Konidaris^a, N. Thompson^a, P. Karkanas^b, E. Panagopoulou^c, K. Harvati^a

^a*Paläoanthropologie, Senckenberg Centre for Human Evolution and Palaeoenvironment, Eberhard Karls Universität Tübingen, Rümelinstr. 23, 72070 Tübingen, Germany*

^b*Malcolm H. Wiener Laboratory for Archaeological Science, American School of Classical Studies at Athens, Greece*

^c*Ephoreia of Palaeoanthropology-Speleology of Greece, Athens, Greece*

Abstract

Recent excavations at the Middle Pleistocene open-air site of Marathousa 1 have unearthed in one of the two investigated areas (Area A) a partial skeleton of a single individual of *Elephas (Palaeoloxodon) antiquus* and other faunal remains in spatial and stratigraphic association with lithic artefacts. In Area B, a much higher number of lithic artefacts was collected, spatially and stratigraphically associated with other faunal remains. The two areas are stratigraphically correlated, the main fossiliferous layers representing an *en masse* depositional process in a lake margin context. Evidence of butchering (cut-marks) has been identified on two bones of the elephant skeleton, as well on other mammal bones from Area B. However, due to the secondary deposition of the main find-bearing units, it is of primary importance to evaluate the degree and reliability of the spatial association of the lithic artefacts with the faunal remains. Indeed, spatial association does not necessarily imply causation, since natural syn- and post-depositional processes may equally produce spatial association. Assessing the degree and extent of post-depositional reworking processes is crucial to fully comprehend the archaeological record, and therefore to reliably interpret past human behaviours. The present study uses a comprehensive set of spatial statistics in order to disentangle the depositional processes behind the distribution of the archaeological and palaeontological record at Marathousa 1. Preliminary results of our analyses suggest minor reworking and substantial spatial association of the lithic and faunal assemblages, supporting the current interpretation of Marathousa 1 as a butchering site.

Keywords: Spatial analysis, Site formation processes, Vertical distribution, Fabric analysis, Point pattern analysis, Middle Pleistocene

*Corresponding author

Email address: domenico.giusti@uni-tuebingen.de (D. Giusti)

1 **1. Introduction**

2 Archaeological site formation processes, intensively studied since the early 1970s
3 ([Isaac, 1967](#); [Schiffer, 1972, 1983, 1987](#); [Shackley, 1978](#); [Wood and Johnson, 1978](#);
4 [Binford, 1981](#); [Schick, 1984, 1986, 1987](#); [Petraglia and Nash, 1987](#); [Petraglia and](#)
5 [Potts, 1994](#), among others), “still insufficiently taken in consideration” ([Texier, 2000](#),
6 p.379) at the beginning of the 21st century, are nowadays fully acknowledged in the ar-
7 chaeological practice ([Villa, 2004](#); [Bailey, 2007](#); [Brantingham et al., 2007](#); [Malinsky-](#)
8 [Buller et al., 2011](#); [Vaquero et al., 2012](#); [Bargalló et al., 2016](#), among others). Drawing
9 inferences about past human behaviours from scatters of archaeological remains must
10 account for syn- and post-depositional contextual processes.

11 Several methods are currently applied in order to qualify and quantify the type and
12 degree of reworking of archaeological assemblages. Within the framework of a geoar-
13 chaeological and taphonomic approach, spatial statistics offer meaningful contributions
14 in unravelling site formation and modification processes from spatial patterns. How-
15 ever, while the spatio-temporal dimension is an ineluctable inherent property of any
16 biotic and abiotic process, spatial statistics are still insufficiently applied.

17 Distribution maps are cornerstones of the archaeological documentation process
18 and are primary analytic tools. However, their visual interpretation is prone to subjec-
19 tivity and is not reproducible ([Bevan et al., 2013](#)). Since the early 1970's (see [Hodder](#)
20 and [Orton \(1976\)](#); [Orton \(1982\)](#) and references therein), the traditional, intuitive, ‘eye-
21 balling’ method of spotting spatial patterns has been abandoned in favour of more ob-
22 jective approaches, extensively borrowed from other fields. Nevertheless, quantitative
23 methods, while still percolating in the archaeological sciences from neighbouring dis-
24 ciplines, are not extensively used. Moreover, only a relatively small number of studies
25 have explicitly applied spatial point pattern analysis or geostatistics to the study of site
26 formation and modification processes ([Lenoble et al. \(2008\)](#); [Domínguez-Rodrigo et al.](#)
27 ([2014b,a, 2017](#)); [Carrer \(2015\)](#); [Giusti and Arzarello \(2016\)](#); [Organista et al. \(2017\)](#) -
28 but see [Hivernel and Hodder \(1984\)](#) for an earlier work on the subject).

29 The goal of a taphonomic approach to spatial analysis is to move beyond distri-
30 bution maps by applying a comprehensive set of multiscale and multivariate spatial
31 statistics in order to reliably construct inferences from spatial patterns. An exhaustive
32 spatial analytic approach to archaeological inference, combined with a taphonomic
33 perspective, is essential for evaluating the depositional processes and integrity of the
34 archaeological assemblage, and consequently for a reliable interpretation of past hu-
35 man behaviours.

36 The present study uses a comprehensive set of spatial statistics in order to disentan-
37 gle the depositional processes behind the spatial distribution of the archaeological and
38 palaeontological record recovered during excavation at the Middle Pleistocene open-air
39 site of Marathousa 1, Megalopolis, Greece ([Panagopoulou et al., 2015](#); [Harvati et al.](#),
40 [2016](#)).

41 **1.1. Marathousa 1**

42 The site (Fig. 1), discovered in 2013 at the edge of an active lignite quarry (?), is
43 located between two lignite seams in the Pleistocene deposits of the Megalopolis basin,
44 Marathousa Member of the Choremi Formation ([van Vugt et al., 2000](#)). The regular

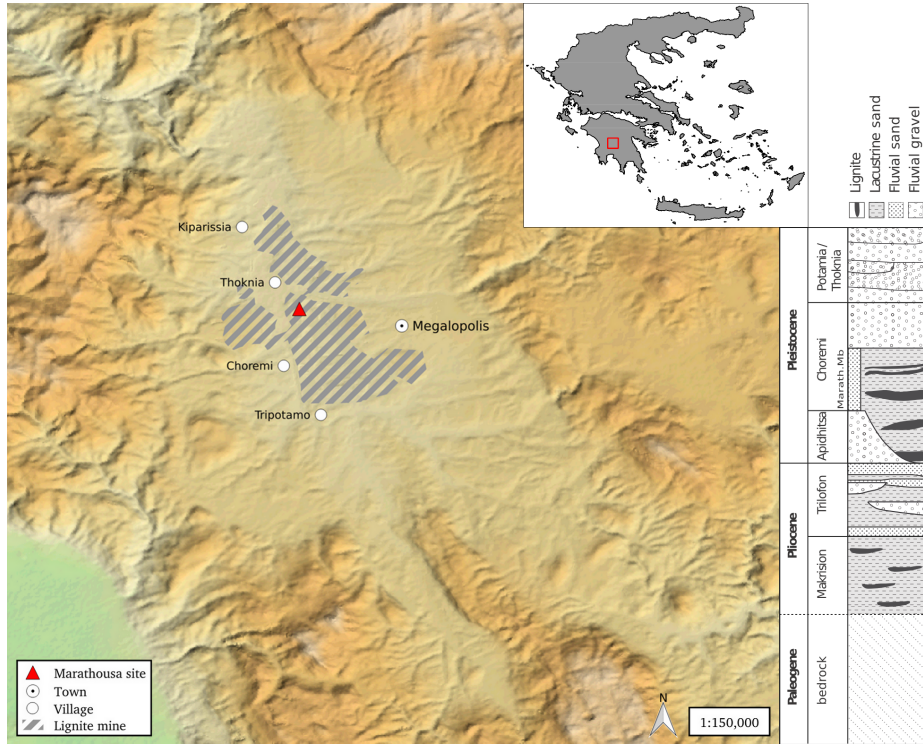


Figure 1: Geographical location of the Marathousa 1 site in the Megalopolis basin and stratigraphic column of the basin, modified after [van Vugt et al. \(2000\)](#).

45 alternation of lacustrine clay, silt and sand beds with lignite seams has been interpreted
 46 having cyclic glacial (or stadial) and interglacial (or interstadial) origin ([Nickel et al., 1996](#)). The half-graben configuration of the basin, with major subsidence along the
 47 NW-SE trending normal faults along the eastern margin, resulted in the gentle dip of
 48 the lake bottom at the opposite, western, margin of the lake, enabling the formation of
 49 swamps and the accumulation of organic material for prolonged periods of time ([van
 50 Vugt et al., 2000](#)).

51 Two excavation areas have been investigated since 2013 (Fig. 2): Area A, where
 52 several skeletal elements of a single individual of *Elephas (Palaeoloxodon) antiquus*
 53 have been unearthed, together with a number of lithic artefacts; and Area B, located
 54 60 m to the South along the exposed section, where the lithic assemblage is richer and
 55 occurs in association with a faunal assemblage composed of isolated elephant bones,
 56 cervids and carnivores among others ([Konidaris et al., this issue](#); [Tourloukis et al., this issue](#)). Evidence of butchering (cut-marks) have been identified on two of the
 57 elephant bones from Area A, as well on elephant and other mammal bones from Area
 58 B ([Konidaris et al., this issue](#)).

59 The sedimentary sequence of the site (Fig. 3) includes lacustrine and fluvio-lacustrine
 60 clastic deposits between lignite seam II (UA7-UB10) and the lower part of seam III

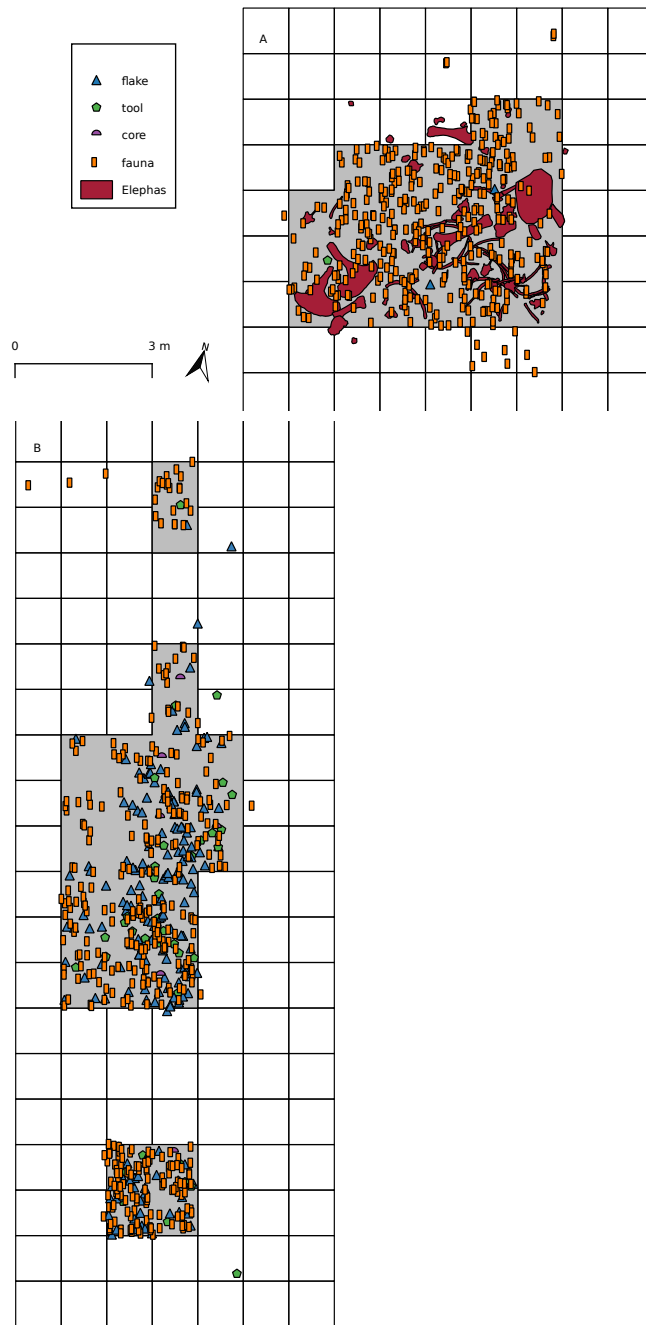


Figure 2: Distribution maps of the remains in Area A and Area B. Grey zone marks the 2015 excavation areas. Area B is located 60 m to the South, along the exposed section of the lignite quarry.

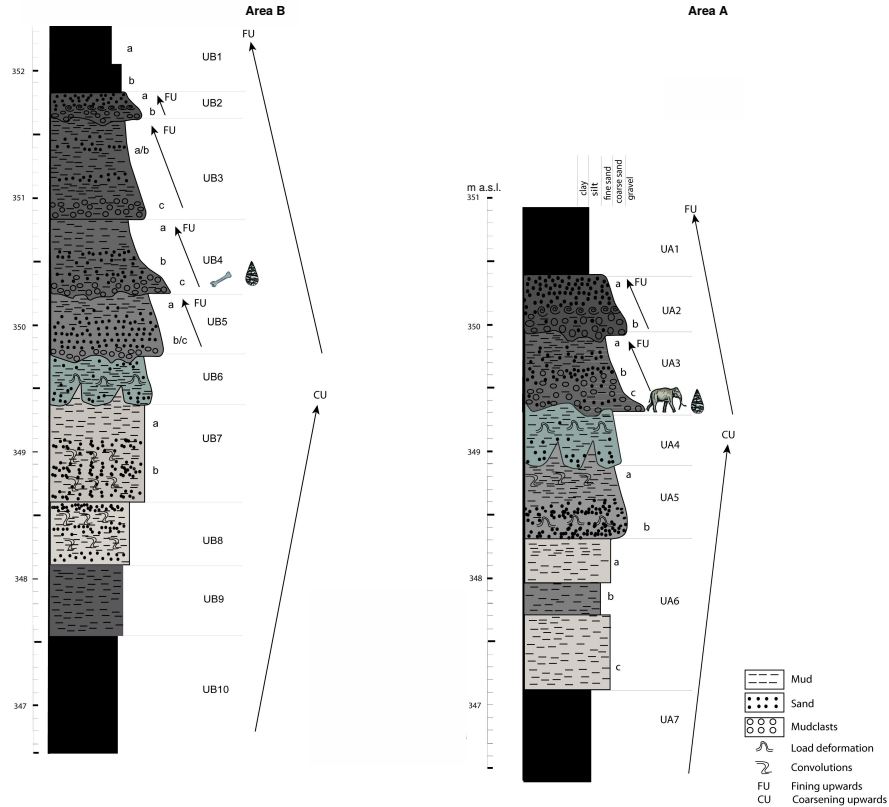


Figure 3: Stratigraphic setting of the Marathousa 1 site, modified after Karkanas et al. (this issue).

(UA1-UB1) (Karkanas et al., this issue; Tourloukis et al., this issue). A major hiatus (UA3/4, UB5/6), attributed to exposure and erosion of a lake shore mudflat, divides the sequence in two parts. The lower part is characterized by relatively high rate subaqueous sedimentation of bedded sands and silts, containing low organic and carbonate content. The upper one is characterized by a series of erosional bounded depositional units, attributed to subaerial organic- and carbonate-rich mudflows and hyperconcentrated flows (Karkanas et al., this issue).

The erosional contacts UA3c/4 and UB4c/5a separate the two main find-bearing units in both areas. In Area A, the elephant remains lie at the contact of UA3c/4 and are covered by UA3c (Fig. 4a); while in Area B, most of the remains were collected from unit UB4c (Fig. 4b). Units UA3c and UB4c (organic- and intraclast-rich silty sands) resemble dilute mudflows, showing a chaotic structure of rip-up clasts from the underlying unit, small-to-large wood fragments and rare rock clasts. In Area B, a relatively low number of remains was also found in massive organic-rich silty sands (UB5a), which locally overlay channalized sands (UB5b/c), probably not preserved in



Figure 4: Photograph (2017) of the left femur of the *Elephas (Palaeoloxodon) antiquus*, lying at the UA3c/4 contact and covered by unit UA3c (a). West profile (2014) of the excavation Area B (square 932/603), exposing the UB4c/5a and UB5c/6 erosional contacts (b).

78 Area A (Karkanas et al., this issue).

79 The flow event described above (units UA3c and UB4c), and specifically the ero-
80 sional contacts between the fossiliferous horizons in the two areas (UA3c/4 and UB4c/5a),
81 provide the essential background for the analysis and interpretation of the spatial dis-
82 tributions at Marathousa 1.

83 The secondary depositional nature of the main find horizons raises the question of
84 how reliable is the spatial association between the lithic artefacts and the partial skele-
85 ton of a single *Elephas (Palaeoloxodon) antiquus* individual and other faunal remains.
86 Since spatial association does not necessarily imply causation, and consequently syn-
87 chrony, the answer has important consequences for the interpretation of the site in the
88 broader context of the Middle Pleistocene human-proboscidean interactions. We aim
89 to tackle this question and disentangle the formation processes acting at Marathousa 1
90 on the basis of spatial patterns through a three-prong spatial analytic approach:

- 91 1. by analysing, in a frame of references, the orientation patterns of remains from
92 relevant stratigraphic units;
93 2. by quantifying and comparing their relative vertical distributions;
94 3. by identifying spatial trends in either the assemblage intensities and the associa-
95 tions between classes of remains.

96 Two contrasting hypotheses are tested: the autochthonous hypothesis (*sensu* Fernández-
97 López, 1991; Domínguez-Rodrigo et al., 2012) states that the flow event, represented
98 by units UA3c and UB4c, eroded and scoured the exposed surface (where the elephant

99 was lying), thereby entraining clastic material (including artefacts) and re-depositing
100 (*sensu* Fernández-López, 1991) this material at a close distance. This model implies the
101 loss of any original, pristine spatial relations between remains, but minor transport from
102 the primary depositional *loci*. On the other hand, the allochthonous hypotheses (*sensu*
103 Fernández-López, 1991; Domínguez-Rodrigo et al., 2012) implies significant transport
104 from the original *loci* of deposition and re-elaboration (*sensu* Fernández-López, 1991).
105 According to this model, the spurious spatial association between the lithic artefacts
106 and faunal remains does not support any behavioural interpretation.

107 **2. Material and methods**

108 Since 2013, systematic investigation of the Marathousa 1 site has been carried out
109 by a joint team from the Ephoreia of Palaeoanthropology-Speleology (Greek Ministry
110 of Culture) and the University of Tübingen. A grid system of 1 square meter units
111 was set up, oriented -14 degrees off the magnetic North, and including the two areas
112 of investigation. The excavation of the deposit proceeded in 50x50 cm sub-squares
113 in Area B and 1x1 m squares in Area A, and spits of 5 to 10 cm thickness, respec-
114 tively. Systematic water-screening of sediments was carried out on-site using 1 mm
115 sieves in order to guarantee recovery of the small-size fraction (e.g., micro-artefacts,
116 small mammal remains, fish, molluscs and small fragments of organic and inorganic
117 material). The three-dimensional coordinates of finds (i.e., all the lithic artefacts, teeth
118 and diagnostic bones; bones and organic material with a-axis \geq 20 mm), collected
119 spits of sediment, samples and geological features (e.g., erosional contacts and mud
120 cracks) were recorded with a Total Station. Dense clouds of surface points of the ele-
121 phant skeletal elements were acquired using both a Total Station and a close-range
122 photogrammetric technique.

123 The dimensions (length, width and thickness) of registered finds were measured
124 on-site with millimetre rules. Orientation (plunge and bearing) of elongated particles
125 (i.e., faunal remains, large wood fragments and lithic artefacts) was recorded since
126 2013 using a clock-like system (the bearing was measured, relatively to the grid North,
127 in twelve clockwise intervals of 30°; the plunge with a 22.5° accuracy). In 2015, the
128 use of a compass and inclinometer with an accuracy of 1° was introduced in Area B to
129 gradually replace the former method.

130 The widespread use of a compass and inclinometer to record orientation data (Voorhies,
131 1969; Fiorillo, 1991; Bertran and Texier, 1995; Bertran et al., 1997; Lenoble and
132 Bertran, 2004; Eberth et al., 2007; Eren et al., 2010; Benito-Calvo et al., 2011; Domínguez-
133 Rodrigo et al., 2012; Domínguez-Rodrigo and García-Pérez, 2013; Domínguez-Rodrigo
134 et al., 2014c; Cobo-Sánchez et al., 2014; Organista et al., 2017, among others) was
135 favoured over the alternative use of a total station (Kluskens, 1990; Dibble et al., 1997;
136 McPherron, 2005; Enloe, 2006; Bernatchez, 2010, among others), mostly due to the
137 time-restricted conditions of the rescue excavation conducted at Marathousa 1.

138 Measurements of the bearing (azimuth) and plunge (dip) of elongated finds were
139 taken along the symmetrical longitudinal a-axis (SLA) of bones (Domínguez-Rodrigo
140 and García-Pérez, 2013), lithic artefacts (Bertran and Texier, 1995) and wood frag-
141 ments (Macdonald and Jefferson, 1985), using the lowest endpoint of the a-axis as an
142 indicator of the vector direction.

143 Other major axes have been alternatively used with the recent application of GIS
144 techniques to retrieve orientation data from secondary source (i.e., excavation photo-
145 graphs, drawings or maps) (Boschian and Saccà, 2010; Benito-Calvo and de la Torre,
146 2011; de la Torre and Benito-Calvo, 2013; Walter and Trauth, 2013; García-Moreno
147 et al., 2016; Sánchez-Romero et al., 2016). However, the experimental works of Domínguez-
148 Rodrigo and García-Pérez (2013) and Domínguez-Rodrigo et al. (2014c) showed that
149 the SLA, defined as the major axis which symmetrically divide the bone, is more accu-
150 rate in determining the preferential orientation of anisotropic assemblages. This a-axis
151 is widely used in taphonomic studies (Toots, 1965; Voorhies, 1969; Eberth et al., 2007;
152 Domínguez-Rodrigo et al., 2012, 2014a; Aramendi et al., 2017, among others) and, as
153 the artefact major axis (Krumbein, 1941), in studies which employ a sedimentologi-
154 cal approach to archaeological fabric (Bertran and Texier, 1995; Bertran et al., 1997;
155 Lenoble and Bertran, 2004; Benito-Calvo et al., 2009, among others).

156 The present study focuses on the excavated stratigraphic units in which most of the
157 archaeological and palaeontological remains were recovered in both excavation areas,
158 namely in UA3c and UA4 in Area A, and UB4c and UB5a in Area B. From the total,
159 subset samples of material were used for each specific spatial analysis. For the fabric
160 analysis we included material collected until 2016. For the vertical distribution and
161 point pattern analyses, the region of investigation was limited to the squares excavated
162 from 2013 until 2015, 25 and 29 square meters respectively in each area.

163 The analyses were performed in R statistical software (R Core Team, 2017). In
164 order to make this research reproducible (Marwick, 2017; Marwick et al., 2017), a
165 repository containing a compendium of data, source code and text is open licensed and
166 available at the DOI: [10.5281/zenodo.822273](https://doi.org/10.5281/zenodo.822273)

167 2.1. Fabric analysis

168 The taphonomic study of the orientation pattern of elongated sedimentary particles,
169 including bones and artefacts, first addressed by Voorhies (1969); Isaac (1967); Bar-
170 Yosef and Tchernov (1972); Schick (1986), more recently led to a noteworthy develop-
171 ment of methods and propagation of applications in Palaeolithic site formation studies
172 (Bertran and Texier, 1995; Bertran et al., 1997; Lenoble and Bertran, 2004; Lenoble
173 et al., 2008; McPherron, 2005; Benito-Calvo et al., 2009, 2011; Benito-Calvo and de la
174 Torre, 2011; Bernatchez, 2010; Boschian and Saccà, 2010; Domínguez-Rodrigo et al.,
175 2012; Domínguez-Rodrigo and García-Pérez, 2013; Domínguez-Rodrigo et al., 2014c;
176 de la Torre and Benito-Calvo, 2013; Walter and Trauth, 2013; García-Moreno et al.,
177 2016; Sánchez-Romero et al., 2016, among others).

178 Fabric analysis can provide valuable insight into site formation and taphonomic
179 processes, allowing discrimination between different orientation patterns (isotropic,
180 linear or planar) associated with a range of sedimentary processes. Whereas water-flow
181 deposits are generally characterized by relatively good sorting and preferred orientation
182 of clasts parallel, or normal to the flow direction (linear fabric) (Petruglia and Potts,
183 1994); debris-flow deposits mostly exhibit massive, poorly bedded mixtures of un-
184 sorted sediments and random orientation of clasts (isotropic fabric), except at the flow
185 margins where linear fabric may occur (Pierson, 2005). On the other hand, undisturbed
186 archaeological sites, as well as experimental sites, have been observed to have planar
187 fabric (Bertran et al., 1997; Lenoble and Bertran, 2004). Nevertheless, grey zones exist

188 between depositional processes, so that an unequivocal discrimination based only on
189 fabric observations is often not possible, and other taphonomic criteria must also be
190 considered (Lenoble and Bertran, 2004). As an example, while overland flows (runoff)
191 have been observed to show planar fabrics (Lenoble and Bertran, 2004), anisotropy
192 without significant transport can be caused in a lacustrine floodplain by low-energy pro-
193 cesses such as lake transgression and regression, as well as water-sheet flows formed
194 during rainy seasons (Cobo-Sánchez et al., 2014).

195 At the margin of a lacustrine environment, relatively close to the surrounding re-
196 lief, a combination of high- and low-energy processes can be expected. According to
197 the sedimentological and micromorphological study of the Marathousa 1 site, mud-
198 flows and hyperconcentrated flows are associated with the main find-bearing horizons
199 (Karkanas et al., this issue). Hyperconcentrated flows are intermediate states, defined
200 by sediment concentration, in the continuum between subaerial water flows and debris
201 flows. Benvenuti and Martini (2002) reported that, when a turbulent hyperconcentrated
202 flow expands over a surface - as in the case of Marathousa 1 - a two-phase flow may
203 develop, with a more concentrated, coarser grained bottom flow-layer (traction carpet)
204 moving slower than the upper turbulent flow-layer carrying washload and suspended
205 load. Resultant deposit may exhibit diagnostic inverse grading, or a continuously ag-
206 grading bed. Parallel or normal orientation of the clast to the flow direction can be
207 observed (Benvenuti and Martini, 2002). Moreover, a simulation model showed that
208 linear fabric can develop in mudflows as well. However, after deposition, settling of the
209 clasts may affect the fabric to some extent, depending on the viscosity of the mudflow
210 (Lindsay, 1968).

211 As part of our three-prong spatial analytic approach, we conducted comparative
212 fabric analysis with the aim to investigate the dynamics of the depositional processes
213 at Marathousa 1.

214 Since fabric strength has been found to be positively correlated with the shape and
215 size of the clast, for the fabric analysis we subset samples of remains with length \geq 2 cm
216 and elongation index (the ratio length/width) $I_e \geq 1.6$ (Lenoble and Bertran, 2004). The
217 samples are listed in Table 1 and include mostly wood fragments and faunal remains
218 from the four stratigraphic units under investigation. Bones have been found to readily
219 react to water flow and show very early anisotropic patterns (Domínguez-Rodrigo et al.,
220 2014c). Flume experiments showed that wood fragments as well tend to align parallel
221 to the current direction (Macdonald and Jefferson, 1985). No distinction of skeletal
222 elements was made, both due to the high fragmentation rate of faunal remains in Area
223 B, and because recent experiments showed a similar orientation pattern for different
224 bone shapes (Domínguez-Rodrigo et al., 2012; Domínguez-Rodrigo and García-Pérez,
225 2013).

226 The sample of bones belonging to the individual of *Elephas (P.) antiquus* from
227 Area A was analysed separately and included the humerus, ulna, femur and tibia; the
228 atlas, axis and 16 complete vertebrae or vertebral fragments; 29 complete ribs or rib
229 fragments; 2 calcanea; 4 metatarsals/metacarpals; the pyramidal; the trapezoid and the
230 pelvis. The sample from UB5a was too small (only 7 observations) and was there-
231 fore excluded. In order to asses the reliability of the orientation data recorded using
232 the clock method, we separately analysed two sub-samples from unit UB4c, selected
233 from a set of finds recorded using both methods. All the sampled observations are

Table 1: List of sampled observations for the fabric analysis.

Sample	<i>n</i>	Type		
		Fauna	Wood	Lithic
UA3c	49	23	25	1
UA4	38	8	30	-
<i>E. (P.) antiquus</i>	63			
UB4c	38	30	1	7

representative of the whole study area.

Rose diagrams and uniformity tests, such as Rayleigh, Kuiper, Watson and Rao tests (Jammalamadaka et al., 2001), were used to visualise and evaluate circular isotropy in the sample distribution. The Rayleigh test is used to assess the significance of the sample mean resultant length (\bar{R}), assuming that the distribution is unimodal and not bi- or plurimodal. The \bar{R} ranges from 0 to 1: values close to 1 indicate that the data are closely clustered around the mean direction; when the data are evenly spread \bar{R} has a value close to 0. A p – value lower than 0.05 rejects the hypothesis of uniformity with a 95% confidence interval. Kuiper, Watson and Rao are omnibus tests used to detect multimodal departures from circular uniformity. The Watson's goodness of fit test was conducted for the von Mises distribution (circular normal distribution). The test results are evaluated against critical values: a result higher than the critical value rejects with confidence the null hypothesis.

Randomness testing of three-dimensional data was conducted with the Woodcock S_1/S_3 test (Woodcock and Naylor, 1983). Considering both the plunge and bearing of the oriented items, this method, based on three ordered eigenvalues (S_1, S_2, S_3), is able to discriminate the shape and strength of the distributions. The shape parameter $K = \frac{\ln(S_1/S_2)}{\ln(S_2/S_3)}$ ranges from zero (uni-axial girdles) to infinite (uni-axial clusters). The parameter $C = \ln(S_1/S_3)$ expresses the strength of the preferential orientation, and its significance is evaluated against critical values from simulated random samples of different sizes. A perfect random uniform distribution would have $C = 0$ and $K = 1$.

The Benn diagram (Benn, 1994) adds to the Woodcock test an isotropy ($IS = S_3/S_1$) and an elongation ($ES = 1 - (S_2/S_1)$) index. Like the former method, it is able to differentiate between linear (cluster), planar (girdle) or isotropic distributions. There are no published raw data from actualistic studies on hyperconcentrated flows or other depositional processes affecting the orientation of bones and artefacts deposited on lacustrine floodplains (but see Morton (2004) and Cobo-Sánchez et al. (2014) as pioneer studies on this subject). However, we included in the Benn diagram references to published results from observation of fabrics in modern subaerial slope deposits, i.e., debris flow and runoff (Bertran et al., 1997; Lenoble and Bertran, 2004).

2.2. Vertical distribution

The vertical distribution of materials has been long investigated with the aim of identifying cultural levels, by visually interpreting cross-sectional plots. However, recent advances in GIS techniques allow to inspect at higher resolution the three-dimensional distributions of archaeological remains (McPherron et al., 2005; Anderson and Burke, 2008, among others).

Table 2: List of sampled observations for the vertical distribution and point pattern analyses.

Sample	<i>n</i>	Lithic class					Faunal class			
		Debris/chip	Flake	Bone flake	Tool	Core	Indet.	Bone	Tooth	Microfauna
UA3c	279	46	2	-	1	-	1	171	14	44
UA4	61	3	1	-	-	-	-	45	4	8
UB4c	1243	753	154	1	34	6	2	246	28	19
UB5a	101	50	12	-	3	-	-	30	3	3

In analysing the vertical dispersion of material at Marathousa 1, we provisionally assume that a general concentration of unsorted lithic artefacts and faunal remains in the proximity of the erosional surfaces would support an autochthonous origin of the assemblages; whereas a homogeneous vertical distribution of remains from the UA3c and UB4c units would suggest an allochthonous origin, significant transport and subsequent redeposition of the material. Indeed, massive process such as mudflows or hyperconcentrated flows, have high erosional power and rather chaotic structure, which may result in inverse or normal grading (Benvenuti and Martini, 2002).

In order to estimate the degree of vertical dispersion while controlling for the size of the archaeological material, dimensional classes were set up following typological criteria. Lithic artefacts were classified as debris/chips when smaller than a cutoff length of 15 mm (Tourloukis et al., this issue). Other classes include flakes, tools and cores; the latter being the bigger and heavier debitage product. Table 2 summarises the sample size for each class. Lithic debris/chips constitute the larger part of the assemblage from UB4c (60%) and UB5a (49%); whereas in Area A they represent only a moderate percentage in the upper UA3c unit (16%). The very rare presence of lithic artefacts in the underlying unit UA4 is nevertheless significant. In this unit, the faunal remains are also found in much lower numbers, their number reduced to one fourth of those found in UA3c. For the point pattern analysis (see below), we used the same subset of material for both excavation areas.

For Area B, the material recovered from the water-screening was randomly provenanced according to the 5 cm depth of the excavated spit and the coordinates of the 50x50 cm quadrant of the excavation square. Following the same excavation protocol, the same procedure was applied for the water-screened material of Area A, which was randomly provenanced according to 3D-coordinates of the 1x1 m excavation square and 10 cm spit.

Ordinary Kriging interpolation of the recorded points of contact between the UA3c/UA4 and the UB4c/UB5a stratigraphic units were used to reconstruct the UA3c/4 and UB4c/5a erosional surfaces (Fig. 5a,b). In geostatistics, Kriging is a method of interpolation which, from a modelled function of spatial autocorrelation between known points (e.g., recorded elevations), calculates values of unknown points (e.g., predicted elevations). Thus, in order to address our specific objective, i.e., to quantify and analyse the vertical distribution of the archaeological and palaeontological material, we measured the minimum orthogonal distance of each specimen to the interpolated erosional surface (Fig. 5c). For the units above and below this surface (i.e., UB4c and UB5a), the relative distribution of lithic classes and faunal remains was informally tested by means of kernel density estimations.

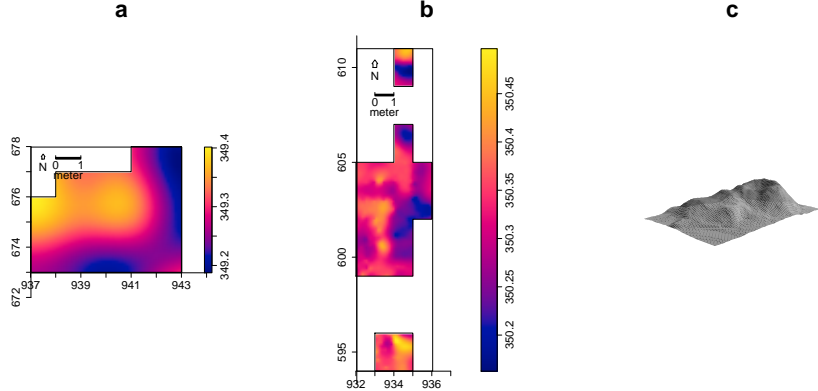


Figure 5: Ordinary Kriging interpolation of the UA3c/4 (a) and UB4c/5a (b) erosional surface; the color scale denotes elevation a.s.l. Illustration of the method used to quantify the vertical dispersion of remains with respect to the UA3c/4 (a) and UB4c/5a (b) surface.

In Area A, the UA3c/4 erosional surface is mixed, rather than sharp: remains of the eroded unit UA4 are mixed with pockets of the UA3c organic-rich silty sands and intraclast-rich mudflows (Karkanas et al., this issue). However, from sparse known points of the erosional contact, the UA3c/4 surface was interpolated and the vertical dispersion of remains estimated as well. The elephant remains were excluded from this analysis, since they clearly lie horizontally at the UA3c/4 contact (Fig. 4a and SI).

Finally, a Student's two sample t-test allowed us to compare the empirical distributions of different groups of remains for each stratigraphic unit.

2.3. Point pattern analysis

A spatial point pattern is defined as the outcome of a random spatial point process (repetitions of it would always create a different pattern). The observed patterns of the archaeological and palaeontological remains were treated as manifestations of spatial point processes, i.e., site formation processes. Point pattern analysis investigates the spatial arrangement of points with the aim of identifying spatial trends. In order to integrate the previous studies of the fabric and vertical distributions, we directed our point pattern analysis equally to the intensity of the patterns (the rate of occurrence of the recorded finds) and to the spatial interaction between different types of finds.

As the average number of random points per unit area, intensity informs about homogeneity or inhomogeneity in the distribution of events (e.g., clasts) generated by a point process (e.g., mudflow), i.e., whether the rate of occurrence is uniform or spatially varying across the study area. Intensity, usually non-parametrically evaluated by means of kernel density estimation (Diggle, 1985), was assessed for the distribution of material from the UB4c, UB5a and UA3c units. Cross-validation bandwidth, which assumes a Cox process, and edge correction were applied using the methods described in Diggle (1985).

In the presence of a covariate, it is recommended to further investigate the dependence of intensity on that explanatory variable (Baddeley et al., 2012). In order to evaluate whether variation in the density of materials was correlated to the topography of the erosional surface, we computed a local likelihood smoothing estimate of the intensity of remains from UB4c as a function of the UB4c/5a surface elevation model. Formal tests enabled us to assess the evidence of that dependence and to quantify the strength of the covariate. The Kolmogorov-Smirnov test of CSR (Complete Spatial Randomness) and Berman's Z_2 statistics were used to test the strength of evidence for a covariate effect. The Receiver Operating Characteristic (ROC) plot, and the area under the ROC curve (AUC), closely related to Berman's Z_2 test, measure the magnitude of the covariate effect. AUC values close to 1 or 0 indicate strong discrimination, whereas intermediate values (0.5) suggest no discrimination power.

Intensity, evaluated by means of kernel density maps, although informative and widespread in the literature, nonetheless does not provide sufficient information to reliably infer about site formation processes.

Whereas intensity is a first-order property of the point process, multiscale inter-point interaction is measured by second or higher-order moment quantities, such as the Ripley's K correlation function (Ripley, 1976, 1977) and the distance G -, F - and J -functions. Three different types of inter-point interaction are possible: random, regular or cluster. In a hypothesis-testing framework, pointwise envelopes are computed by a number of random simulations of the null hypothesis (i.e., random/Poisson distribution). Thus, values of the empirical distribution (black solid line) are plotted against the benchmark value (red dotted line) and the envelopes (grey area) which specify the critical points for a Monte Carlo test (Ripley, 1981). Regular patterns are assumed to be the result of inhibition processes, while cluster patterns are the result of attraction processes.

In order to test the spatial interaction between remains associated with the erosional event of UB4c and those associated with the underlying UB5a unit, we treated the data as a multivariate point pattern, assuming that the point patterns in UB4c and UB5a are expressions of two different stationary point processes, i.e., depositional events. We performed a cross-type pair correlation function ($g_{ij}(r)$), derivative of the multitype $K_{ij}(r)$ function, which is the expected number of points of type j lying at a distance r of a typical point of type i . The function is a multiscale measurement of the spatial dependence between types i (UB4c) and j (UB5a). Randomly shifting in 199 Monte Carlo permutations each of the two patterns, independently of each other, estimated values of $\hat{g}_{ij}(r)$ are compared to a benchmark value $g_{ij}(r) = 1$, which is consistent with independence or at least with lack of correlation between the two point processes.

In addition to the pair correlation function, the multitype nearest-neighbour $G_{ij}(r)$ function was used to estimate the cumulative distribution of the distance from a point of type i (UB4c) to the nearest point of type j (UB5a). It measures the spatial association between the two assemblages. For the cross-type G -function, the null hypothesis states that the points of type j follow a Poisson (random) distribution in addition to being independent of the points of type i .

Thus, in a randomisation technique, when the solid line of the observed distribution ($\hat{G}_{ij}(r)$ or \hat{g}_{ij}) is above or below the shaded grey area, the pattern is significantly consistent with clustering or segregation, respectively. In order to reduce the edge effect

378 bias in estimating the correlation between points, we implemented Ripley's isotropic
379 edge correction (Ohser, 1983; Ripley, 1988).

380 Complete spatial randomness and independence (CSRI) of the two point processes
381 (UB4c and UB5a) would support an allochthonous origin hypothesis for the assem-
382 blage recovered from the UB4c unit. According to the allochthonous model, the mas-
383 sive, chaotic UB4c flow event randomly re-elaborated the material embedded in it,
384 independently from the material deposited in UB5a. On the other hand, positive or
385 negative association can be interpreted as expressions of different autochthonous pro-
386 cesses.

387 Similarly, the particle size horizontal distribution of the lithic assemblage from
388 UB4c was investigated by means of a transformation of the multitype K -function
389 ($K_{i\bullet}(r) - K(r)$, see Baddeley et al. (2015), p.608). In this case, we treated the data
390 as the manifestation of a single multitype point process. In a joint distribution analysis,
391 the locations and types of points are assumed to be generated at the same time. The null
392 model of a random labelling test states that the type of each point is determined at ran-
393 dom, independently of other points, with fixed probabilities. The multitype K -function
394 was estimated for a subset of possible combinations of coupled classes of remains, and
395 evaluated against the envelope of 199 Monte Carlo permutations.

396 Whereas the null hypothesis of randomness is consistent with an allochthonous
397 model, spatial clustering or segregation would support an autochthonous model. Specif-
398 ically, the close occurrence of small specimens, such as lithic debris/chips, with larger
399 dimensional classes of remains would suggest the lack of sorting by natural deposi-
400 tional processes predating the UB4c flow event (when the UB5a surface was exposed).
401 On the other hand, spatial segregation would suggest the action of sorting processes,
402 such as winnowing.

403 As for the three-dimensional distribution of the lithic artefacts in Area A, and their
404 spatial association with the partial skeleton of the *E. (P.) antiquus*, we applied three-
405 dimensional univariate and bivariate second-order functions. A rectangular box of 20
406 square meters and 80 cm vertical extent was selected for the analyses (green outline in
407 Fig. 11a). Assuming homogeneity, the univariate pair correlation function ($g_3(r)$) was
408 estimated for the pattern of all the artefacts (mostly debris/chips) from UA3c and UA4.

409 In the specific context of the site, complete spatial randomness (CSR) would sug-
410 gest that the pattern most probably is the result of a random distribution process, such
411 as a high energy mass movement, thus supporting an allochthonous model of depo-
412 sition. On the other hand, spatial aggregation would support a primary origin of the
413 assemblage. Nevertheless, topography and natural obstructions may generate spatial
414 clustering as well.

415 In support to the pair correlation function, the cross-type nearest-neighbour func-
416 tion has been applied in order to compute, for each artefact recovered from the UA3c
417 and UA4 units, the nearest point of the three-dimensional clouds of points associated
418 with the elephant skeleton. A prevalence of short distances would indicate aggregation
419 of the lithic artefacts around the mass of the elephant; whereas a uniform or symmetric
420 distribution would support the action of random independent processes

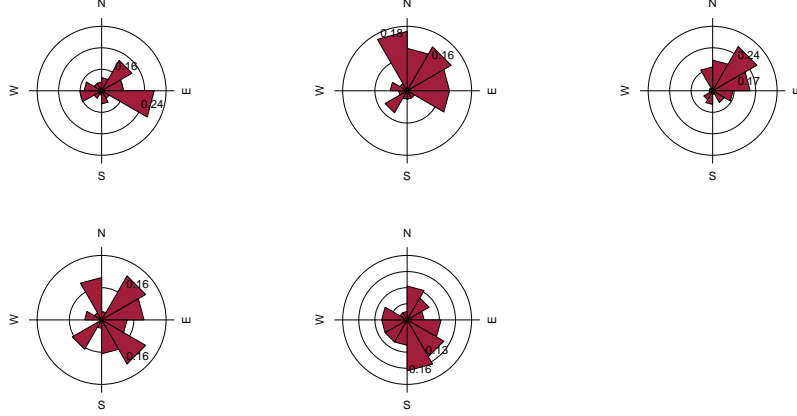


Figure 6: Rose diagrams showing the bearing patterns of samples from UA3c (a), UA4 (b), the elephant carcass (c) and UB4c (d: clock method, e: compass method).

Table 3: Value and p – value of circular uniformity test statistics.

Sample	mean dir.	Rayleigh		Kuiper		Watson		Rao	
		\bar{R}	p	V_n	p	U^2	p	U	p
UA3c	77.17°	0.268	0.029	2.4698	<0.01	0.2967	<0.01	271.8367	<0.001
UA4	35.79°	0.386	0.003	2.5656	<0.01	0.3437	<0.01	246.3158	<0.001
<i>E. (P.) antiquus</i>	54.64°	0.489	2.775e-07	3.4811	<0.01	0.906	<0.01	291.4286	<0.001
UB4c (clock)	91.66°	0.276	0.054	1.8963	0.01 < p < 0.025	0.1937	0.025 < p < 0.05	255.7895	<0.001
UB4c (compass)	151.17°	0.243	0.106	1.3944	>0.15	0.1268	>0.10	128.5263	>0.10

3. Results

3.1. Fabric analysis

The rose diagrams in Fig. 6 visualise the circular distributions of the examined specimens. Overall, the UA4 sample and the sample of elephant bones show unimodal distributions with predominant peaks in the NE quadrant; while the ones from units UA3c and UB4c suggest multimodal distributions. Specifically, the UA4 sample distribution (Fig. 6b) spreads largely in the NE quadrant. Similarly, the circular distribution of the elephant sample (Fig. 6c), mainly lying in UA4, resembles the former distribution: it is skewed to the SW and concentrated in the NE quadrant. On the other hand, the UA3c sample (Fig. 6a) shows a bimodal distribution with two peaks to the E and NE, and the two samples from Area B (Fig. 6d,e) suggest a different multimodal scenario uniformly distributed.

Table 3 summarises the results of the circular uniformity tests. With regard to the UA3c sample, the Rayleigh test (p – value = 0.03) rejected the null hypothesis of circular uniformity. The mean resultant length ($\bar{R} = 0.27$) and the mean direction of 77° are thus significant, assuming the distribution is unimodal. However, the rose diagram (Fig. 6a) showed a bimodal distribution. The Kuiper, Watson and Rao omnibus tests, more powerful than the Rayleigh test in detecting multimodal deviation from uniformity, also rejected the null hypothesis of uniformity, therefore suggesting significant

440 anisotropy in the distribution.

441 For the UA4 sample and the subset of elephant bones, all the uniformity tests agreed
442 in rejecting the null hypothesis in favour of a preferentially oriented distribution. The
443 Elephant sample, with respect to the other, showed significantly higher test results,
444 thus stronger anisotropy. As suggested by the rose diagrams (Fig. 6c), this sample has
445 a mean direction towards the NE (55°) and relatively low circular variance (29°).

446 The UB4c sub-samples had discordant test results when considering the omnibus
447 statistics. However, according to the Rayleigh test, the mean resultant lengths (\bar{R})
448 and the mean directions were not significant for both sub-samples of measurements:
449 $p - values > 0.05$ failed to reject the null hypotheses of isotropy with 95% confidence
450 interval. This result is well confirmed by the Kuiper, Watson and Rao tests for the
451 sub-sample of measurements recorded using the compass. Conversely, the omnibus
452 tests failed to reject the hypotheses of uniformity for the other sub-sample of measure-
453 ments recorded with the clock method. The rose diagram (Fig. 6d) suggested for the
454 latter distribution strong multimodality, with uniformly spread peaks. The contrasting
455 results obtained for the UB4c sub-samples are most probably due to the shape of those
456 distributions. Indeed, the clock system, being less accurate, tends to produce a less
457 dense distribution, more subject to show a multimodal shape when the distribution is
458 actually uniform (Fig. 6a,d).

459 The Woodcock eigenvalues ratio graph (Fig. 7a) presents the shape (K) and strength
460 (C) of the distributions. Fig. 7b plots confidence levels of Monte-Carlo critical C val-
461 ues, varying for sample sizes. The two sub-samples from Area B nearly overlapped,
462 thus suggesting reliability of the orientation measurements collected using the clock
463 system, although of low accuracy. The two sub-samples, together with the UA3c sam-
464 ple, having low C values, plotted close to the origin of the ratio graph. Therfore, they
465 indicate weak preferential orientation (UA3c) and significant randomness (UB4c). On
466 the other hand, the UA4 and the elephant samples, with higher C values, showed a
467 stronger and significant tendency to orient preferentially. The shape parameter K of
468 the samples varied from $K = 0.25$ for the UB4c sample measured with the compass,
469 to $K = 0.66$ for the one measured with the clock, to $K = 48$ for the elephant sample.
470 Overall, all the samples, except the UA3c one ($K = 1.63$), plotted below the average
471 shape value ($K = 1$) between girdles and clusters distributions.

472 The Benn diagram (Fig. 8) resembles the Woodcock ratio graph (Fig. 7a). The
473 samples from units UB4c and UA3c clearly plotted at a distance from the UA4 and the
474 elephant samples. The UB4c samples plotted in the upper corner of the ternary graph,
475 with the UB4c sub-sample of measurements taken with the compass exhibiting more
476 isotropy. The UA3c sample, with an elongation index similar to the elephant sample,
477 but higher isotropix index, plotted towards the centre. Compared to the ranges of fab-
478 rics recorded for modern natural processes (debris flow, runoff), the fabric from the
479 UA3c and UB4c units plotted well inside the cluster of debris flows, with the UB4c
480 (comp) sample suggesting even more random orientations. On the other hand, the
481 sample of elephant remains, which lie mostly on UA4 and are covered by UA3c, plot-
482 ted significantly close to the sample from unit UA4. They both presented the lowest
483 isotropy index (IS), but not high elongation index (EL). Thus, they plotted in the
484 average between linear and planar orientations, at the margins of the range of runoff
485 processes. Yet they still plotted within the cluster of debris flows fabrics. Moreover,

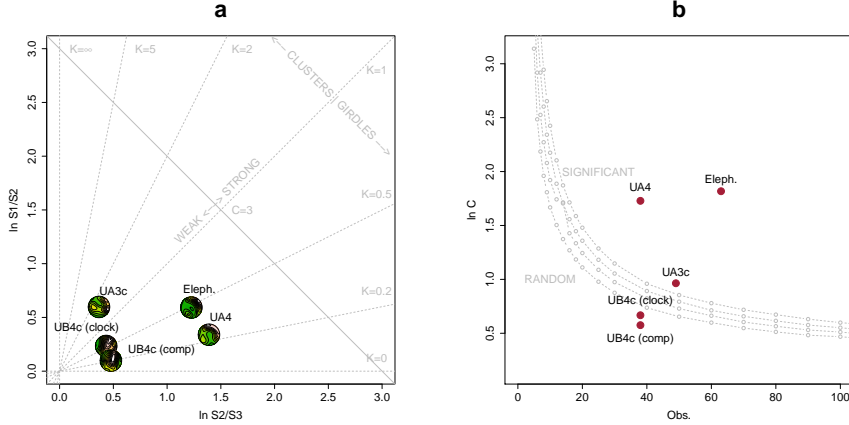


Figure 7: Woodcock's eigenvalues ratio graph (a) and plot of the Monte-Carlo critical S_1/S_3 test values, for varying sample sizes and confidence levels (b), modified from [Woodcock and Naylor \(1983\)](#).

as suggested also by the uniformity tests (Tab. 3), the elephant sample showed a more linear attitude with respect to the UA4 sample.

3.2. Vertical distribution

Fig. 9 compares the distribution of the absolute elevations of the partial skeleton of the *Elephas (P.) antiquus* with the other remains from Area A. Overall, the vertical distribution of the elephant approximates a normal distribution with mean (μ) 349.25 m a.s.l. and standard deviation (σ) 0.12 m. The mean elevation of the erosional contact between the two stratigraphic units is slightly above the latter ($\mu = 349.30$ m). Although difficult to quantify due to its mixed nature, the range of elevations of this contact, as estimated from the IDW interpolation (Fig. 9a), is relatively small ($\sigma = 0.06$ m).

Three lithic artefacts (two flakes and one tool) from the UA3c unit are located within its positive half. Only one flake has been found in the lower UA4, at about 349.10 m, together with three chips. However, they plotted well within the left tail of the debris/chip distribution from the unit above. Despite the scarcity ofdebitage products in this area, waste products (debris/chip) are relatively well represented (16% of the UA3c sample). Their vertical distribution approximates a normal distribution ($\mu = 349.50$ m and $\sigma = 0.18$ m), having almost 50% of the sample in the range of elevations of the erosional surface and the rest above it. Notably, the distribution of the faunal remains from the same unit resembles that of the debris/chip. The Welch two sample t-test ($p - value = 0.5099$) failed to reject the null hypothesis that the two population means are equal. On the other hand, the vertical distribution of faunal remains recovered from the UA4 unit is comparable with that of the *Elephas* ($p - value = 0.6562$). Nevertheless, the density functions altogether clearly confirm one of the main observations assessed during excavation, namely that the elephant remains and most of the recovered faunal and lithic material in Area A lie at or close to the UA3c/4 contact, with unit UA3c covering the remains.

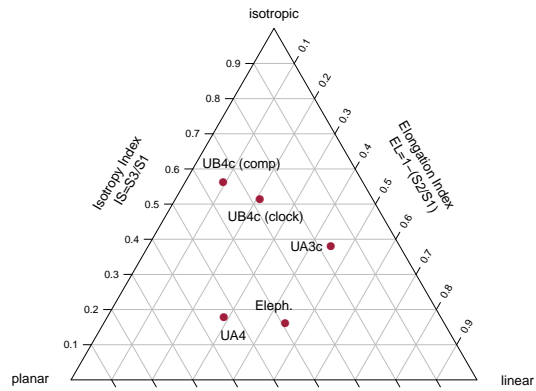


Figure 8: Benn's diagram. Fabric ranges of natural processes modified from Bertran et al. (1997); Lenoble and Bertran (2004).

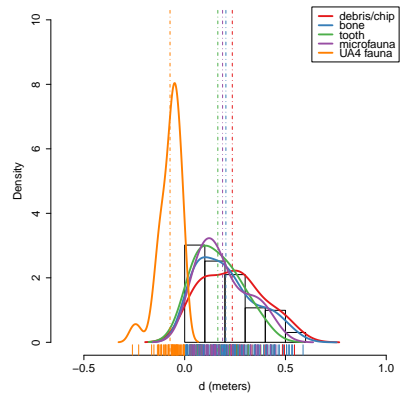


Figure 9: Empirical density functions of minimum orthogonal distances (d) to the UA3c/4 surface. The histogram represents the total distribution of remains from UA3c; dashed lines indicate mean values.

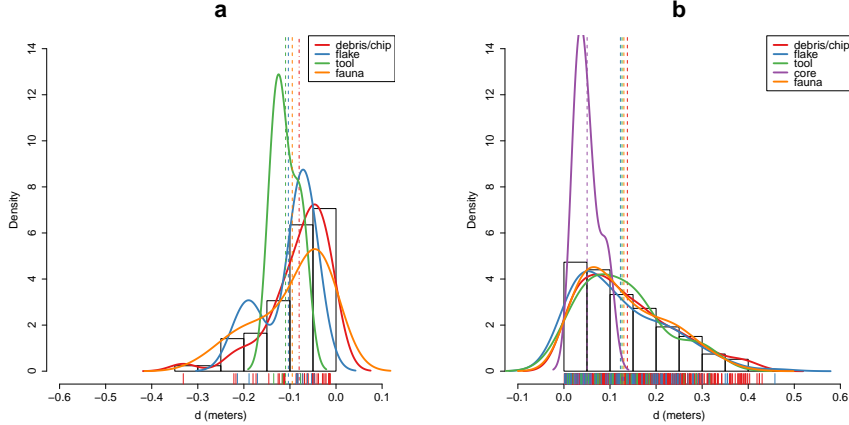


Figure 10: Empirical density functions of minimum orthogonal distances (d) to the UB4c/5a surface. The histogram represents the total distribution of remains from UB5a (a) and UB4c (b); dashed lines indicate mean values.

Fig. 10 shows the empirical density functions of the minimum distances from each specimen from Area B to the UB4c/5a erosional contact (Fig. 5b). The combined distribution of any type of find from the UB5a unit (Fig. 10a) skewed to the left with a short tail (up to -0.3 m). The mode, between 5 and 10 cm below the roof of UB5a, indicates a general concentration of material very close to the contact of this unit with the overlying UB4c, in accordance with the mean distribution of the different classes of remains. Although the majority of both the lithic and faunal assemblages were found in the uppermost 15 cm of UB5a, few debris/chips and bone fragments occur lower in the sequence, yet no more than 30 cm below the roof of this unit. Very few flakes, three tools and no cores have been found in this unit. As a whole, the lithic assemblage from UB5a, mostly composed by debris/chips, is only 7% of the most conspicuous assemblage from UB4c.

The global distribution of unit UB4c was right skewed (up to almost 0.6 m) and centred at about 5 cm above the contact with the underlying unit UB5a (Fig. 10b). Almost 30% of the sample fell exactly at the erosional contact that separates UB4c from UB5a. The density estimations of the lithic debris/chip, flakes, tools and faunal remains significantly overlap, whereas the distribution of the six cores shows a bimodal shape with peaks at 5 and 20 cm above the contact. However, the Welch Two Sample t-test of the lithic and faunal sample means failed to reject the null hypothesis ($p\text{-value} = 0.6295$).

3.3. Point pattern analysis

Results of the point pattern analysis are complementary to those obtained from the analysis of the vertical and fabric distributions.

Regarding Area A, kernel density estimation and three-dimensional functions were applied in order to quantitatively depict the spatial distribution of the lithic assemblage

537 in relation to the elephant skeleton.

538 Fig. 11a shows the smoothing kernel intensity estimation of the faunal assemblage
539 from the UA3c unit. Contour lines delimit the density of the lithic sample. The partial
540 skeleton of the *E. (P.) antiquus* is superimposed on it. A preliminary visual examination
541 of the plot suggests a homogeneous distribution of lithics (mostly debris/chips) and
542 fossils. Spots of higher density appear to be spread around and in association with the
543 elephant remains.

544 The univariate pair correlation function of the joined lithic assemblage from the
545 UA3c and UA4 units (Fig. 11b) suggests aggregation of finds. The estimated $\hat{g}_3(r)$
546 function (black solid line) wanders above the benchmark value (red dotted line) until
547 values of $r = 0.8$. However, for distances between 35 and 65 cm, it lies above the
548 grey envelope of significance for the null hypothesis of CSR, indicating that at those
549 distances artefacts occur closer than expected in the case of random processes. For
550 values of $r > 0.8$, the function stabilises at values close to 0, suggesting a Poisson
551 distribution. The plot illustrates the random distribution of finds between patches of
552 clusters that we observe in the kernel density estimation (Fig. 11a).

553 The histogram in Fig. 11c shows the density of the distances calculated from each
554 artefact to the nearest-neighbour elephant remain. A right skewed distribution, with
555 a prevalent peak at 10 cm and mean $\mu = 30$ cm is an indication of the relatively strong
556 aggregation of events around the mass of the elephant skeleton.

557 As for Area B, the analysis first focused on the spatial distribution and cross-
558 correlation of the assemblages from UB4c and UB5a (Fig. 12); and secondly on the
559 interaction between classes of remains from UB4c (Fig. 13).

560 Figs. 12a,b respectively show kernel density estimations of the combined lithic and
561 faunal assemblages from both the units analysed. Despite the samples size difference,
562 a first visual examination suggests the presence of interesting spatial structures.

563 Regarding the UB4c unit (Fig. 12a), the high density of material concentrated
564 around the western square 934/600 suggests that the pattern could have been the re-
565 sult of an inhomogeneous, non-uniform depositional process. Visual comparison of
566 the density plot with the elevation model of the erosional contact between the UB4c
567 and UB5a units (Fig. 5b) suggests positive correlation between lower elevations (topo-
568 graphic depressions) and higher density of remains. Fig. 12c shows the results of the
569 ρ -function, which estimates the intensity of the UB4c sample assemblage as a func-
570 tion of the covariate underlying topography created by the erosional event. Within the
571 range of elevation between 350.2 and 350.4 m, the occurrence of finds is higher and
572 the intensity decreases with the rise of elevation, i.e., finds are more likely to be found
573 at lower elevations than would be expected if the intensity was constant.

574 Spatial Kolmogorov-Smirnov and Berman's Z_2 (Berman, 1986) statistics were used
575 in order to test the dependence of the UB4c pattern on the covariate erosional sur-
576 face. Both KS ($D = 0.11952$, $p - \text{value} = 7.772e - 16$) and Z_2 ($Z_2 = -7.8447$,
577 $p - \text{value} = 4.34e - 15$) significantly rejected the null hypothesis of CSR. Although
578 the tests suggested evidence that the intensity depends on the covariate, the effect of
579 the covariate is weak and it seems to have no discriminatory power. The ROC curve
580 and AUC statistics (0.56), which measure the strength of the covariate effect, suggest
581 that the underlying UB4c/5a topography does not completely explain the localised high
582 density of occurrence in the UB4c.

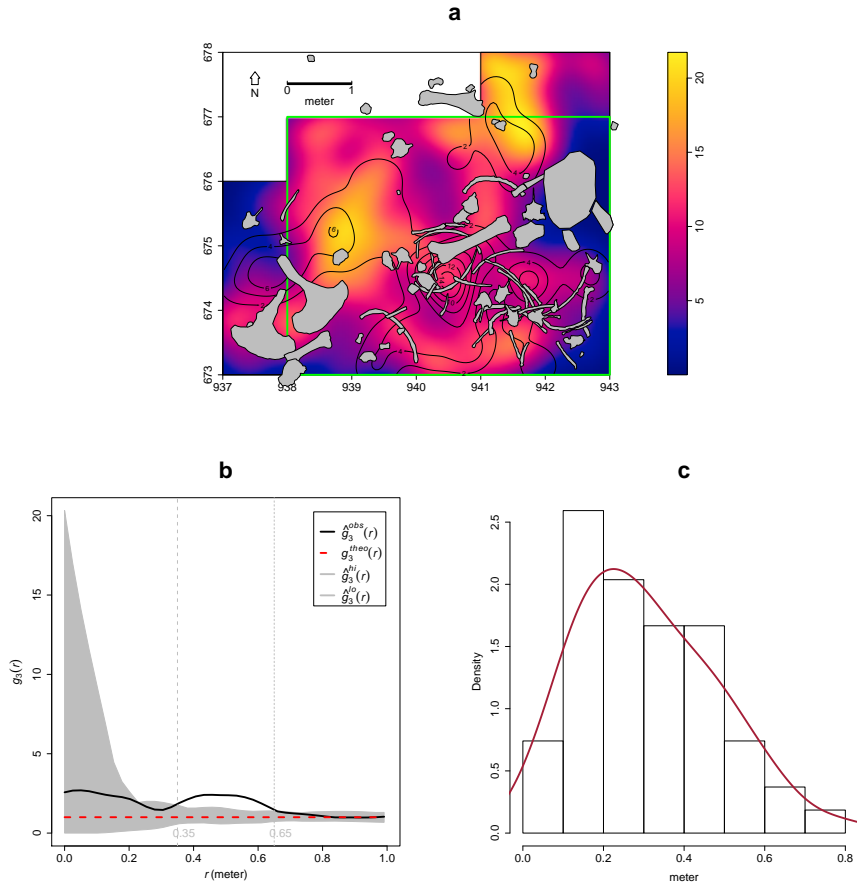


Figure 11: Kernel smoothed intensity function of the lithic and faunal assemblages from UA3c. Isolines mark the density of the lithic artefacts (a). Pair correlation function ($g_3(r)$) of a three-dimensional pattern of lithic artefacts from UA3c and UA4. Grey envelope of 999 Monte Carlo simulations under the CSR null hypothesis (b). Three-dimensional distance from each lithic artefact from UA3c and UA4 to the nearest neighbour elephant remain (c).

583 Relative spatial segregation seems to occur between the assemblages from UB4c
584 (Fig. 12a) and UB5a (Fig. 12b), with high density of the former distribution corre-
585 sponding to low density of the latter. The former analysis of the vertical distribution
586 showed that the two assemblages occur very close to their stratigraphic contact. In
587 order to further investigate the spatial interaction between the two depositional events,
588 we applied multitype pair correlation ($g_{ij}(r)$) and nearest-neighbour ($G_{ij}(r)$) functions.

589 Fig. 12d shows the estimated values of the multivariate $\hat{g}_{ij}(r)$ function against the
590 envelope of the null hypothesis, obtained by randomly shifting the position of remains
591 from the two distributions in 199 Monte Carlo simulations. For fixed values of r less
592 than 30 cm the observed function lies below the benchmark value of independence, thus
593 indicating segregation; but it wanders at the lower edge of the grey envelope. For fixed
594 distances of $r > 0.3$ m the observed and theoretical lines significantly overlap. Overall,
595 the function suggests independence of the two point processes (UB4c and UB5a) at
596 multiple scales.

597 However, the estimated $\hat{G}_{ij}(r)$ function (Fig. 12c), running well below the signifi-
598 cience grey envelope for fixed values of $r > 0.3$ m, confirms that the nearest-neighbour
599 distances between remains from UB4c and UB5a are significantly longer than expected
600 in the case of independent processes. Interestingly, at values of $r < 0.2$ m the observed
601 function failed to reject the null hypothesis of Complete Spatial Randomness and In-
602 dependence (CSRI).

603 With the aim to integrate the vertical distribution analysis, the particle size spatial
604 distribution of remains from the UB4c unit were investigated by means of a deriva-
605 tive of the multitype K -function, randomly labelling the classes of remains. Fig.13
606 shows a selection of the array of possible combinations between classes. In any panel,
607 the estimated function wanders above the benchmark value. Such positive deviations
608 from the null hypotheses suggest that debris/chips are more likely to be found close
609 to the other class of remains than would be expected in case of a completely random
610 distribution. Permutating the lithic debris/chips with flakes (Fig.13a), tools (Fig.13b),
611 cores (Fig.13c) and faunal remains (Fig.13d), the Monte Carlo test results would have
612 been significantly consistent with clustering, if we had chosen distance values $r > 0.4$,
613 $r > 0.4$, $r > 0.9$, $r > 0.8$, respectively. Conversely, we could not reject the null
614 hypothesis of CSRI for lesser values of r .

615 4. Discussion

616 Recent excavations at the Middle Pleistocene site of Marathousa 1 have unearthed
617 in one of the two investigated areas (Area A) a partial skeleton of a single individual of
618 *Elephas (P.) antiquus*, whose bones are in close anatomical association, and spatially
619 and stratigraphically associated with lithic artefacts and other faunal remains. In Area
620 B, 60 m to the South of Area A, we collected a much higher number of lithic artefacts
621 (Tourloukis et al., this issue), spatially and stratigraphically associated with other fau-
622 nal remains, including isolated elephant bones, cervids and carnivores among others
623 (Konidaris et al., this issue).

624 The two areas are stratigraphically correlated, the main fossiliferous layers (UA3c
625 and UB4c) representing a massive depositional process, such as a hyperconcentrated
626 flow that dumped material in a lake margin context (Karkanas et al., this issue).

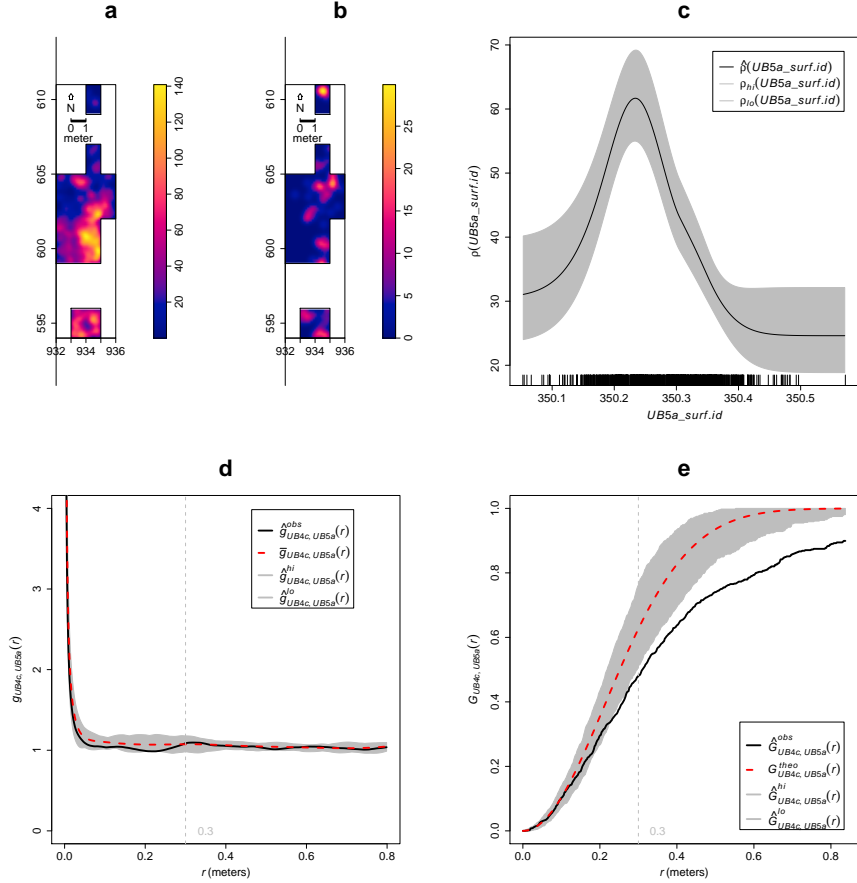


Figure 12: Kernel smoothed intensity function of the lithic and faunal assemblages from UB4c (a) and UB5a (b). Smoothing estimate of the intensity of remains from UB4c, as a function of the erosional surface UB4c/5a. Grey shading is pointwise 95% confidence bands (c). Cross-pattern pair correlation function ($g_{ij}(r)$) between the UB4c and UB5a distributions. Grey envelope of 199 Monte Carlo simulations under the independence of components null hypothesis (d). Multitype nearest-neighbour function ($G_{ij}(r)$) between the UB4c and UB5a distributions (e).

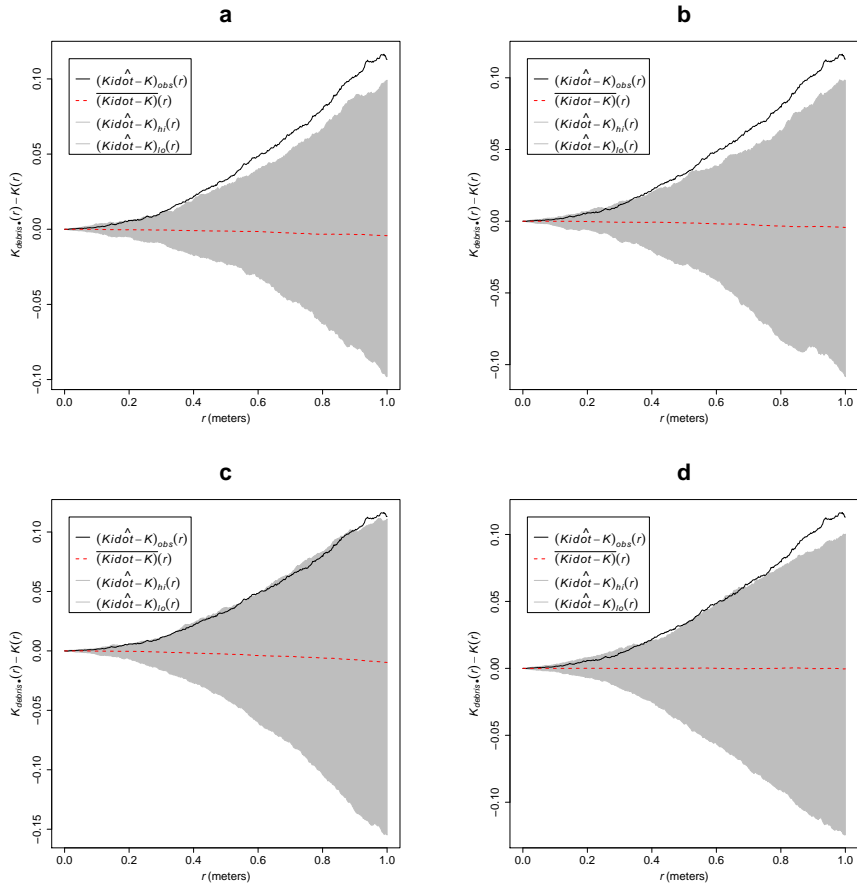


Figure 13: Random labelling test for the UB4c assemblage. Grey pointwise envelope of 199 Monte Carlo permutation of debris/chips with flakes (a); tools (b); cores (c); fossils (d).

627 To date, evidence of butchering (cut-marks) has been identified on two bones of
628 the elephant skeleton from Area A, as well on elephant and other mammal bones from
629 Area B (see Konidaris et al. (this issue)).

630 However, due to the secondary depositional nature of the main fossiliferous horizon,
631 it is of primary importance to evaluate the degree and reliability of the spatial
632 association of the lithic artefacts with the faunal remains, and especially with the ele-
633 phant skeleton. In order to tackle our main objective, we applied a comprehensive
634 set of spatial statistics to the distributions of the archaeological and zooarchaeologi-
635 cal/palaeontological remains from relevant stratigraphic units of the two areas of in-
636 vestigation. Preliminary results of our analyses are here discussed for both areas.

637 *4.1. Fabric analysis*

638 The analysis of the orientation (plunge and bearing) of subsets of remains, mostly
639 bone fragments, organic residues and lithic artefacts, showed different patterns for the
640 two main find-bearing units.

641 The test results (Tab. 3) for the UA4 sample and the sample of elephant remains
642 - which lie on unit UA4 and are covered by UA3c - indicated significant preferential
643 orientations towards the NE (Figs. 6b,c). As shown by the Woodcock's (Fig. 7) and the
644 Benn's diagrams (Fig. 8), these samples plotted together at a distance from the others.
645 Such convergence suggests that the elephant carcass, the other faunal remains and the
646 organic material, deposited on unit UA4, were subject to the same processes.

647 Far from the isotropic corner in the Benn's diagram these two samples from Area
648 A plotted approximately in between the linear and planar extremes, with the elephant
649 sample showing a more planar fabric. When the results published by Bertran et al.
650 (1997) and Lenoble and Bertran (2004) from observations of fabrics in modern sub-
651 aereal slope deposits were used as a reference, the two samples aggregated well within
652 the cluster of runoff process. Yet, they still plotted at the extreme margins of debris
653 flow and relatively distant from the linear corner.

654 This result is consistent with the exposure of unit UA4 to overland water-laden
655 processes that occurred before the flood event UA3c/UB4c (Karkanas et al., this is-
656 sue). Notably, the erosive nature of low-energy processes triggered by rain-water has
657 been observed on lacustrine floodplains, and is associated with anisotropic patterns
658 in autochthonous assemblages (Cobo-Sánchez et al., 2014; Domínguez-Rodrigo et al.,
659 2014c; García-Moreno et al., 2016).

660 On the other hand, the fabric of the UA3c sample, being similar to those of the
661 UB4c sub-samples (Figs. 7 and 8), supports the stratigraphic correlation between these
662 units across the two investigated areas. The fabric analysis suggests that the UA3c/UB4c
663 process can be categorized as a flood event, which falls in between the spectrum of de-
664 bris and hyperconcentrated flow???. Indeed, random distribution and orientation of
665 clasts is expected for debris flows, except at flow margins, where preferential orienta-
666 tion and clusters of clasts have been observed (Pierson, 2005).

667 Unlike bones with a tubular shape (i.e., long bones), ribs and vertebrae are prone
668 to orient preferentially under high energy processes, less likely under low energy pro-
669 cesses (Domínguez-Rodrigo and García-Pérez, 2013; Domínguez-Rodrigo et al., 2014c).
670 Interestingly, whereas some of the ribs share the same preferential orientation with the

long bones, others are oriented NW/SE. However, a NW/SE orientation could be consistent with a prevalent NE direction of the flow (and vice-versa), since long bones could roll orthogonally to the flow direction (Voorhies, 1969).

On the other hand, a higher energy flood would lead to an under-representation of most cancellous grease-bearing bones, which are prone to be easily transported by water induced processes (Voorhies, 1969). Yet several carpals, tarsals, metapodials, phalanges, ribs and vertebrae are present and in close spatial association with the elephant cranium and other skeletal elements.

The presence of many of the skeletal elements suggests that the elephant carcass was not subjected to high energy processes . Thus, we can assume that relatively low energy overland flows slightly reworked and oriented the exposed elements of the already dismembered (and probably already marginally displaced) elephant carcass, which mostly preserves close anatomical associations, but not anatomical connections.

In Area B, two sub-samples from the same stratigraphic unit were analysed, according to the different methods used for recording the orientation (plunge and bearing) of the finds (i.e., 'clock' vs. compass), mostly faunal remains, wood fragments and lithic artefacts. Due to the different shapes of the two distributions (Figs. 6d,e), test statistics reported contrasting results (Tab. 3). Indeed, the clock system, recording non-continuous circular data, tends to produce a distribution more subject to show a multimodal shape when the distribution is actually uniform. However, the three-dimensional Woodcock (Fig. 7) and Benn (Fig. 8) diagrams agreed upon assessing the randomness of the samples. Despite minor differences between the two samples, both plotted with the UA3c sample in the reference range of debris flows.

4.2. Vertical distribution

As for the vertical distribution, we assume that mass wasting processes, such as debris or hyperconcentrated flows, would predominantly distribute extremely poorly sorted clasts homogeneously throughout the sequence. Normal or inverse grading can be observed in such flows (Pierson, 2005). A concentration of unsorted elements in the proximity of the erosional surface, as well as the absence of any grading, would in turn suggest an autochthonous assemblage.

The lithic assemblage from Area A - the combined sample from units UA3c and UA4 ($n = 54$), composed by a fewdebitage products and a relatively high number of debris/chips and retouch waste products (Tab. 2) - plotted predominantly in the proximity of the erosional surface created by the UA3c/UB4c event. The faunal remains from unit UA3c resemble the distribution of the archaeological assemblage as a whole; whereas the ones from the underlying unit UA4 match the vertical distribution of the elephant (Fig. 9).

Overall, the material recovered from unit UA3c did not show any grading and mainly plotted at the bottom of the unit, thus is consistent with the hypothesis of an autochthonous assemblage.

In Area B, two samples from units UB4c ($n = 1243$) and UB5a ($n = 101$) respectively, were analysed (Tab. 2) for quantifying the minimum orthogonal distance of each item to the modelled erosional surface (Fig. 5b).

The vertical distribution of lithic artefacts and fossils from unit UB4c showed a predominant peak right at the contact with the erosional surface. Almost 30% of this rich

sample plotted at a distance between 0 and 5 cm from the erosional contact; whereas the rest gently skewed to the upper part of the unit, up to about 50 cm. The same distribution was observed for all classes of remains, suggesting no size sorting and an origin very close to the erosional surface (Fig. 10b).

The density distribution of the sample from the underlying UB5a unit (Fig. 10a) globally indicates a more constrained vertical displacement of remains (within 30 cm below the erosional surface). Whereas lithic artefacts and fossils mostly plot right at the contact and just below it, a few debris/chips and faunal remains were found lower in the sequence. No size sorting was observed, but, notably, lithic cores are absent and the debris/chip distribution is wider than the distribution of the few flakes and tools.

Field observations of cracks in the clayey UB5a unit testify to shrinking and swelling during wet and dry cycles (Karkanas et al., this issue), which suggests that vertical displacement of some small lithics and fossil fragments at lower depths with respect to the UB5a/4c contact probably resulted from clay desiccation.

Likewise, Lenoble and Bertran (2004) documented up to 30 cm vertical dispersion and frequent vertical plunge of artefacts from the marshy silty clay of the Croix-de-Canard site, sector 3.

Furthermore, a recent experimental study of animal trampling in water saturated substrates reported negative correlation with artefact size, significant inclination and greater vertical displacement than any former work: a maximum between 16 and 21 cm, with a mean of about 6 cm (Eren et al., 2010).

The fact that the majority of the remains from units UB4c and UB5a plotted at, or very close to the contact between these two layers, the relatively high percentage of lithics in both units, as well as the absence of size sorting or grading, suggest autochthonous assemblages, deposited in UB5a and subsequently eroded *in situ* by the UA3c/UB4c flood event.

4.3. Point pattern analysis

The hypothesis that in both areas the lithic and faunal assemblages were primarily deposited *in situ* and were subsequently reworked by a low energy flood, was further explored by means of point pattern analysis.

We assumed that a completely random spatial distribution of the lithic artefacts and faunal remains would suggest an allochthonous origin and subsequent transport to the site by the action of a random massive process, such as debris flow. Nevertheless, clustering of artefacts is not necessarily evidence of human presence. Aggregation or segregation patterns could be produced by a range of biotic and/or natural processes. Human activities, topography and physical obstructions alike could trigger spatial aggregation.

The three-dimensional distribution of lithic artefacts from unit UA3c shows significant clustering for values of r between 35 and 65 cm. Lithic artefacts occur relatively close to the skeletal elements of the elephant, at a distance between 20 and 50 cm at most (Fig. 11). The richest cluster of about 20 lithic artefacts is located to the SW of the cranium, close to the right femur and the scatter of ribs and vertebrae.

Considering the prevalent NE orientation of the elephant bones and the other faunal remains from UA4, it is not unlikely that a SW/NE oriented flood could have been

760 responsible for the observed accumulation to the SW of the elephant cranium, which
761 would have represented an important obstruction to the flow. A similar case of clus-
762 tering of small remains, apparently dammed by a long elephant tusk, has also been
763 observed at Castel di Guido (Italy) ([Boschian and Saccà, 2010](#)). Secondary deposi-
764 tion by low-energy flows and clustering of artefacts and bones blocked by an aurochs
765 carcass have been as well documented at the site of 'Ein Qashishadd (Israel) ([Hovers](#)
766 [et al., 2014](#)).

767 As mentioned above, whereas fairly random fabric and spatial distribution of coarse
768 clasts are observed at the centre of modern debris flow deposits, preferential orientation
769 and clustering may occur at the margin of the flood ([Pierson, 2005](#)). Yet the fabric
770 analysis of the UA3c sample shows a random distribution, which falls within the range
771 of debris flow (Fig. 8), and the pair correlation function (Fig. 9b) suggests significant
772 clustering of lithic artefacts at relatively small scale: a pattern less likely to be produced
773 by a large scale massive process such as a debris flow. Moreover, clusters of lithic
774 artefacts occur as well in areas with lower densities of elephant bones.

775 Small scale clustering; proximity to the elephant remains and the erosional surface;
776 absence of spatial size sorting and, on the contrary, the presence of a relatively high
777 number of lithic debris/chips associated with some flakes and tools; close anatomical
778 spatial association of the elephant skeletal elements, slightly displaced and preferen-
779 tially oriented: these lines of evidences support the hypothesis of an autochthonous
780 deposition, subject to localised minor reworking.

781 A similar pattern can be observed in Area B, where an initial set of spatial statistics
782 confirmed that the inhomogeneous density of remains from unit UB4c (Fig. 12a) is
783 not completely explained by the covariate effect of the underlying complex topography
784 created by the erosional event UA3c/UB4c (Fig. 5b).

785 Thus, we explored the relative spatial interaction between the UB4c and the un-
786 derlying UB5a samples. We assumed that complete spatial randomness of the two
787 independent depositional processes would occur in case of an exogenous origin and
788 transportation of the UB4c assemblage. The hypothesis of an autochthonous original
789 deposition of the faunal and lithic assemblages on the UB5a unit, subsequently eroded
790 *in situ* by a relatively high energy flood (UB4c), was tested by cross-pattern spatial
791 correlation functions (Figs. 12d,e). Whereas the two samples are vertically adjacent to
792 the erosional surface (Fig. 10), on the horizontal plane they are both more segregated
793 than expected for a random distribution.

794 Moreover, for the UB4c sample, an unsorted particle size spatial distribution was
795 confirmed (Fig. 13). The occurrence in the same place of small and large classes of
796 remains suggests that post-depositional processes, such as water winnowing, have not
797 severely affected the assemblage. Hyperconcentrated flows would have dumped mate-
798 rial onto the lake margin. In this way, particles would have been frozen and deposited
799 *en masse*. Hence their non-sorted spatial distribution.

800 Conversely, the extraordinary preservation and number of mint to sharp, unsorted
801 lithic artefacts from the UB4c unit; their density, positively correlated to the topog-
802 raphy, and significantly segregated from the underlying distribution of remains; the
803 vertical proximity of both assemblages from UB4c and UB5a to the erosional surface;
804 as well as the random orientation pattern of the former, suggest that significant dis-
805 placement of materials due to the erosional event can be excluded.

806 The faunal and lithic assemblages from unit UB4c therefore most likely derived
807 from the local erosion of exposed mudflat areas (UB5a layer) and have been slightly
808 redistributed by the same flood event that capped the elephant in Area A.

809 Further evidence that the recovered assemblage has not undergone substantial re-
810 working and has retained its original characteristics would come from the refitting anal-
811 ysis, currently in progress. To date, 4 bone refits have been found in Area B: three from
812 unit UB4c, respectively at 4.77, 0.05 and 0.01 m distance; and one between two mam-
813 mal bone fragments from units UB4c and UB5a, at a very short distance (0.09 m).
814 Interestingly, one of the elements of the most distant refit (a *Dama sp.* mandibular
815 fragment) shows traces of carnivore gnawing (Konidaris et al., this issue).

816 In conclusion, multiple lines of evidence suggest that the erosional event UA3c/UB4c
817 represents an *en masse* depositional process, i.e. a hyperconcentrated flow, in the con-
818 tinuum between water and debris flow. This flood would have locally reworked at a
819 small scale the already exposed or slightly buried and spatially associated lithic and
820 faunal assemblages.

821 Although the UA3c/UB4c process represents a snapshot of a relatively short time-
822 frame, inferences about the use of space by human groups, in terms of knapping
823 episodes and butchering activities, are unreliable in light of the current information.

824 The spatial pattern observed at the site is indeed the result of the last episode in
825 a palimpsest of spatial processes. Whereas the erosional event represented by the hy-
826 perconcentrated flow UA3c/UB4c caps the sequence and preserves the record, little is
827 known about the eroded underlying occupational horizon.

828 However, whereas hunting or scavenging is still an unsolved matter of debate, con-
829 sidering the rate of bone fragmentation, the density of lithic debris/chips, the number
830 of processed bones and their spatial density and association, it is likely that the assem-
831 blage represents a complex palimpsest of locally repeated events of hunting/scavenging
832 and exploitation of lake shore resources.

833 More data from high resolution excavations in the coming years will allow us to
834 refine the coarse-grained spatio-temporal resolution of our inferences about past human
835 behaviour at Marathousa 1.

836 5. Conclusions

837 At the Middle Pleistocene open-air site of Marathousa 1, a partial skeleton of a
838 single individual of *Elephas (Palaeoloxodon) antiquus* was recovered in stratigraphic
839 association with a rich and consistent lithic assemblage and other vertebrate remains.
840 Cut-marks and percussion marks have been identified on the elephant and other mam-
841 mal bones excavated at the site. The main find-bearing horizon represents a secondary
842 depositional process in a lake margin context.

843 Understanding the site formation processes is of primary importance in order to
844 reliably infer hominin exploitation of the elephant carcass and other animals. To meet
845 this aim, we applied a comprehensive set of multivariate and multiscale spatial analyses
846 in a taphonomic framework.

847 Results from the fabric, vertical distribution and point pattern analyses are consis-
848 tent with a relatively low-energy erosional process slightly reworking at a small scale

849 an exposed (or slightly buried) and consistent scatter of lithic artefacts and faunal re-
850 mains. These results are in agreement with preliminary taphonomic observations of the
851 lithic artefacts ([Tourloukis et al., this issue](#)) and the faunal remains ([Konidaris et al.,](#)
852 [this issue](#)), which also indicate minor weathering and transportation. Our analyses
853 show that multiple lines of evidence support an autochthonous origin of the lithic and
854 faunal assemblages, subject to minor post-depositional reworking. Human activities
855 therefore took place on-site, during an as of yet uncertain range of time.

856 **Acknowledgements**

857 This research is supported by the European Research Council (ERC StG PaGE
858 283503) awarded to K. Harvati. We are grateful to the Municipality of Megalopolis,
859 the authorities of the Region of Peloponnese, and the Greek Public Power corporation
860 (Δ EH) for their support. We also thank Julian Bega and all the participants in the PAGE
861 survey and excavation campaigns in Megalopolis for their indispensable cooperation.

862 **References**

- 863 Anderson, K. L., Burke, A., 2008. Refining the definition of cultural levels at Karabi
864 Tamchin: a quantitative approach to vertical intra-site spatial analysis. *Journal of*
865 *Archaeological Science* 35 (8), 2274–2285.
- 866 Aramendi, J., Uribelarrea, D., Arriaza, M. C., Arráiz, H., Barboni, D., Yravedra, J.,
867 Ortega, M. C., Gidna, A., Mabulla, A., Baquedano, E., Domínguez-Rodrigo, M.,
868 2017. The paleoecology and taphonomy of {AMK} (bed i, olduvai gorge) and its
869 contributions to the understanding of the “zinj” paleolandscape. *Palaeogeography,*
870 *Palaeoclimatology, Palaeoecology*, –.
- 871 Baddeley, A., Chang, Y.-M., Song, Y., Turner, R., 2012. Nonparametric estimation of
872 the dependence of a point process on spatial covariates. *Statistics and Its Interface*
873 5 (2), 221–236.
- 874 Baddeley, A., Rubak, E., Turner, R., 2015. *Spatial Point Patterns: Methodology and*
875 *Applications with R*. Chapman and Hall/CRC, London.
- 876 Bailey, G., 2007. Time perspectives, palimpsests and the archaeology of time. *Journal*
877 *of Anthropological Archaeology* 26 (2), 198 – 223.
- 878 Bar-Yosef, O., Tchernov, E., 1972. On the palaeo-ecological history of the site of Ubei-
879 diya. Vol. 35. Israel Academy of Sciences and Humanities, Jerusalem.
- 880 Bargalló, A., Gabucio, M. J., Rivals, F., 2016. Puzzling out a palimpsest: Testing an
881 interdisciplinary study in level o of abric romaní. *Quaternary International* 417 (Sup-
882 plement C), 51 – 65, advances in Palimpsest Dissection.
- 883 Benito-Calvo, A., de la Torre, I., 2011. Analysis of orientation patterns in Olduvai
884 Bed I assemblages using GIS techniques: Implications for site formation processes.
885 *Journal of Human Evolution* 61 (1), 50 – 60.

- 886 Benito-Calvo, A., Martínez-Moreno, J., Mora, R., Roy, M., Roda, X., 2011. Trampling
887 experiments at Cova Gran de Santa Linya, Pre-Pyrenees, Spain: their relevance for
888 archaeological fabrics of the Upper–Middle Paleolithic assemblages. *Journal of Archaeological Science* 38 (12), 3652–3661.
- 890 Benito-Calvo, A., Martínez-Moreno, J., Pardo, J. F. J., de la Torre, I., Torcal, R. M.,
891 2009. Sedimentological and archaeological fabrics in Palaeolithic levels of the
892 South-Eastern Pyrenees: Cova Gran and Roca dels Bous Sites (Lleida, Spain). *Journal
893 of Archaeological Science* 36 (11), 2566 – 2577.
- 894 Benn, D., 1994. Fabric shape and the interpretation of sedimentary fabric data. *Journal
895 of Sedimentary Research* 64 (4a), 910–915.
- 896 Benvenuti, M., Martini, I. P., 2002. Analysis of terrestrial hyperconcentrated flows and
897 their deposit. In: Martini, I. P., Baker, V. R., Garzón, G. (Eds.), *Flood and Megaflood
898 Processes and Deposits*. Vol. 32 of Special Publication of the International Association
899 of Sedimentologists. Blackwell Publishing Ltd., pp. 167–193.
- 900 Berman, M., 1986. Testing for spatial association between a point process and another
901 stochastic process. *Applied Statistics* 35, 54–62.
- 902 Bernatchez, J. A., 2010. Taphonomic implications of orientation of plotted finds from
903 Pinnacle Point 13B (Mossel Bay, Western Cape Province, South Africa). *Journal of
904 Human Evolution* 59 (3–4), 274 – 288.
- 905 Bertran, P., Hetù, B., Texier, J.-P., Steijn, H. V., 1997. Fabric characteristics of subaerial
906 slope deposits. *Sedimentology* 44 (1), 1 – 16.
- 907 Bertran, P., Texier, J.-P., 1995. Fabric Analysis: Application to Paleolithic Sites. *Journal
908 of Archaeological Science* 22 (4), 521 – 535.
- 909 Bevan, A., Crema, E., Li, X., Palmisano, A., 2013. Intensities, Interactions, and Un-
910 certainties: Some New Approaches to Archaeological Distributions. In: Bevan, A.,
911 Lake, M. (Eds.), *Computational Approaches to Archaeological Spaces*. Left Coast
912 Press, Walnut Creek, pp. 27–52.
- 913 Binford, L. R., 1981. Behavioral archaeology and the "pompeii premise". *Journal of
914 Anthropological Research* 37 (3), 195–208.
- 915 Boschian, G., Saccà, D., 2010. Ambiguities in human and elephant interactions? Sto-
916 ries of bones, sand and water from Castel di Guido (Italy). *Quaternary International*
917 214 (1–2), 3 – 16.
- 918 Brantingham, P. J., Surovell, T. A., Waguespack, N. M., 2007. Modeling post-
919 depositional mixing of archaeological deposits. *Journal of Anthropological Archae-
920 ology* 26 (4), 517 – 540.
- 921 Carrer, F., 2015. Interpreting Intra-site Spatial Patterns in Seasonal Contexts: an Eth-
922 noarchaeological Case Study from the Western Alps. *Journal of Archaeological
923 Method and Theory*, 1–25.

- 924 Cobo-Sánchez, L., Aramendi, J., Domínguez-Rodrigo, M., 2014. Orientation patterns
925 of wildebeest bones on the lake Masek floodplain (Serengeti, Tanzania) and their
926 relevance to interpret anisotropy in the Olduvai lacustrine floodplain. *Quaternary*
927 *International* 322–323 (0), 277 – 284.
- 928 de la Torre, I., Benito-Calvo, A., 2013. Application of GIS methods to retrieve ori-
929 entation patterns from imagery; a case study from Beds I and II, Olduvai Gorge
930 (Tanzania). *Journal of Archaeological Science* 40 (5), 2446–2457.
- 931 Dibble, H. L., Chase, P. G., McPherron, S. P., Tuffreau, A., Oct. 1997. Testing the
932 reality of a "living floor" with archaeological data. *American Antiquity* 62 (4), 629–
933 651.
- 934 Diggle, P., 1985. A kernel method for smoothing point process data. *Applied Statistics*
935 (*Journal of the Royal Statistical Society, Series C*) 34, 138–147.
- 936 Domínguez-Rodrigo, M., Bunn, H., Mabulla, A., Baquedano, E., Uribelarrea, D.,
937 Pérez-González, A., Gidna, A., Yravedra, J., Diez-Martin, F., Egeland, C., Barba,
938 R., Arriaza, M., Organista, E., Ansón, M., 2014a. On meat eating and human evolu-
939 tion: A taphonomic analysis of BK4b (Upper Bed II, Olduvai Gorge, Tanzania), and
940 its bearing on hominin megafaunal consumption. *Quaternary International* 322–323,
941 129–152.
- 942 Domínguez-Rodrigo, M., Bunn, H., Pickering, T., Mabulla, A., Musiba, C., Baque-
943 dano, E., Ashley, G., Diez-Martin, F., Santonja, M., Uribelarrea, D., Barba, R.,
944 Yravedra, J., Barboni, D., Arriaza, C., Gidna, A., 2012. Autochthony and orientation
945 patterns in Olduvai Bed I: a re-examination of the status of post-depositional biasing
946 of archaeological assemblages from FLK North (FLKN). *Journal of Archaeological*
947 *Science* 39 (7), 2116 – 2127.
- 948 Domínguez-Rodrigo, M., Cobo-Sánchez, L., Yravedra, J., Uribelarrea, D., Arriaza, C.,
949 Organista, E., Baquedano, E., 2017. Fluvial spatial taphonomy: a new method for the
950 study of post-depositional processes. *Archaeological and Anthropological Sciences*,
951 1–21.
- 952 Domínguez-Rodrigo, M., Diez-Martín, F., Yravedra, J., Barba, R., Mabulla, A., Baque-
953 dano, E., Uribelarrea, D., Sánchez, P., Eren, M. I., 2014b. Study of the SHK Main
954 Site faunal assemblage, Olduvai Gorge, Tanzania: Implications for Bed II taphon-
955 omy, paleoecology, and hominin utilization of megafauna. *Quaternary International*
956 322–323, 153–166.
- 957 Domínguez-Rodrigo, M., García-Pérez, A., 07 2013. Testing the Accuracy of Different
958 A-Axis Types for Measuring the Orientation of Bones in the Archaeological and
959 Paleontological Record. *PLoS ONE* 8 (7), e68955.
- 960 Domínguez-Rodrigo, M., Uribelarrea, D., Santonja, M., Bunn, H., García-Pérez, A.,
961 Pérez-González, A., Panera, J., Rubio-Jara, S., Mabulla, A., Baquedano, E., Yrave-
962 dra, J., Diez-Martín, F., 2014c. Autochthonous anisotropy of archaeological mate-
963 rials by the action of water: experimental and archaeological reassessment of the

- 964 orientation patterns at the Olduvai sites . *Journal of Archaeological Science* 41 (0),
965 44 – 68.
- 966 Eberth, D. A., Rogers, R. R., Fiorillo, A. R., 2007. A practical approach to the study of
967 bonebeds. In: Rogers, R. R., Eberth, D. A., Fiorillo, A. R. (Eds.), *Bonebeds. Genesis,*
968 *Analysis, and Paleobiological Significance*. The University of Chicago Press, pp.
969 265–332.
- 970 Enloe, J. G., 2006. Geological processes and site structure: assessing integrity at a late
971 paleolithic open-air site in northern france. *Geoarchaeology* 21 (6), 523–540.
- 972 Eren, M. I., Durant, A., Neudorf, C., Haslam, M., Shipton, C., Bora, J., Korisettar,
973 R., Petraglia, M., 2010. Experimental examination of animal trampling effects on
974 artifact movement in dry and water saturated substrates: a test case from South India.
975 *Journal of Archaeological Science* 37 (12), 3010 – 3021.
- 976 Fernández-López, S. R., 1991. Taphonomic concepts for a theoretical biochronology.
977 *Revista Española de Paleontología* 6, 37–49.
- 978 Fiorillo, A. R., 1991. Taphonomy and depositional setting of careless creek quarry (juda-
979 dith river formation), wheatland county, montana, u.s.a. *Palaeogeography, Palaeo-
980 climatology, Palaeoecology* 81 (3), 281–311.
- 981 García-Moreno, A., Smith, G. M., Kindler, L., Pop, E., Roebroeks, W., Gaudzinski-
982 Windheuser, S., Klinkenberg, V., 2016. Evaluating the incidence of hydrological
983 processes during site formation through orientation analysis. A case study of the
984 middle Palaeolithic Lakeland site of Neumark-Nord 2 (Germany). *Journal of Ar-
985 chaeological Science: Reports* 6, 82 – 93.
- 986 Giusti, D., Arzarello, M., 2016. The need for a taphonomic perspective in spatial analy-
987 sis: Formation processes at the Early Pleistocene site of Pirro Nord (P13), Apricena,
988 Italy. *Journal of Archaeological Science: Reports* 8, 235 – 249.
- 989 Harvati, K., Panagopoulou, E., Tourloukis, V., Thompson, N., Karkanas, P., Athanasiou,
990 A., Konidaris, G., Tsartsidou, G., Giusti, D., 2016. New Middle Pleistocene
991 elephant butchering site from Greece. In: *Paleoanthropology Society Meeting*. At-
992 lanta, Georgia, pp. A14–A15.
- 993 Hivernel, F., Hodder, I., 1984. Analysis of artifact distribution at Ngenyem (Kenya):
994 depositional and postdepositional effects. In: Hietala, H., Larson, P. (Eds.), *Intrasite*
995 *Spatial Analysis in Archaeology*. Cambridge University Press, Ch. 7, pp. 97–115.
- 996 Hodder, I., Orton, C., 1976. *Spatial Analysis in Archaeology. New Studies in Archae-
997 ology*. Cambridge University Press, Cambridge.
- 998 Hovers, E., Ekshtain, R., Greenbaum, N., Malinsky-Buller, A., Nir, N., Yeshurun, R.,
999 2014. Islands in a stream? Reconstructing site formation processes in the late Middle
1000 Paleolithic site of 'Ein Qashish, northern Israel. *Quaternary International* 331, 216–
1001 233.

- 1002 Isaac, G. L., 1967. Towards the interpretation of occupation debris: Some experiments
1003 and observations. *Kroeber Anthropological Society Papers* 37 (37), 31–57.
- 1004 Jammalamadaka, S., Sengupta, A., Sengupta, A., 2001. Topics in Circular Statistics.
1005 Series on multivariate analysis. World Scientific.
- 1006 Karkanas, P., Tourloukis, V., Thompson, N., Giusti, D., Panagopoulou, E., Harvati, K.,
1007 this issue. Sedimentology and micromorphology of the lower palaeolithic lakeshore
1008 site marathousa 1, megalopolis basin, greece. *Quaternary International*.
- 1009 Kluskens, S. L., 1990. Orientation and density analysis of stone artefacts at combe-
1010 capelle bas, périgord, france. Master's thesis, University of Pennsylvania.
- 1011 Konidaris, G., Athanassiou, A., Tourloukis, V., Thompson, N., Giusti, D.,
1012 Panagopoulou, E., Harvati, K., this issue. The elephas (palaeoloxodon) antiquus
1013 skeleton and other large mammals from the lower palaeolithic locality marathousa-
1014 1 (megalopolis basin, greece): preliminary results on taxonomy, biochronology,
1015 palaeoecology and taphonomy. *Quaternary International*.
- 1016 Krumbein, W. C., 1941. Measurement and geological significance of shape and
1017 roundness of sedimentary particles. *JOURNAL OF SEDIMENTARY PETROLOGY*
1018 11 (2), 64–72.
- 1019 Lenoble, A., Bertran, P., 2004. Fabric of Palaeolithic levels: methods and implications
1020 for site formation processes. *Journal of Archaeological Science* 31 (4), 457 – 469.
- 1021 Lenoble, A., Bertran, P., Lacrampe, F., 2008. Solifluction-induced modifications
1022 of archaeological levels: simulation based on experimental data from a modern
1023 periglacial slope and application to French Palaeolithic sites. *Journal of Archaeo-
1024 logical Science* 35 (1), 99 – 110.
- 1025 Lindsay, J. F., 1968. The development of clast fabric in mudflows. *Journal of Sedimen-
1026 tary Research* 38 (4), 1242–1253.
- 1027 Macdonald, D. I. M., Jefferson, T. H., 1985. Orientation studies of waterlogged wood;
1028 a paleocurrent indicator? *Journal of Sedimentary Research* 55 (2), 235–239.
- 1029 Malinsky-Buller, A., Hovers, E., Marder, O., 2011. Making time: ‘Living floors’,
1030 ‘palimpsests’ and site formation processes – A perspective from the open-air Lower
1031 Paleolithic site of Revadim Quarry, Israel. *Journal of Anthropological Archaeology*
1032 30 (2), 89 – 101.
- 1033 Marwick, B., 2017. Computational reproducibility in archaeological research: Ba-
1034 sic principles and a case study of their implementation. *Journal of Archaeological
1035 Method and Theory* 24 (2), 424–450.
- 1036 Marwick, B., d'Alpoim Guedes, J., Barton, C. M., Bates, L. A., Baxter, M., Beavan,
1037 A., Bollwerk, E. A., Bocinsky, R. K., Brughams, T., Carter, A. K., Conrad, C.,
1038 Contreras, D. A., Costa, S., Crema, E. R., Daggett, A., Davies, B., Drake, B. L.,
1039 Dye, T. S., France, P., Fullager, R., Giusti, D., Graham, S., Harris, M. D., Hawks, J.,

- 1040 Heath, S., Huffer, D., Kansa, E. C., Kansa, S. W., Madsen, M. E., Melcher, J., Negre,
1041 J., Neiman, F. D., Opitz, R., Orton, D. C., Przystupa, P., Raviele, M., Riel-Salvatore,
1042 J., Riris, P., Romanowska, I., Smith, J., Strupler, N., Ullah, I. I., Vlack, H. G. V.,
1043 VanValkenberg, N., Watrall, E. C., Webster, C., Wells, J., Winters, J., Wren, C. D.,
1044 2017. Open science in archaeology. *SAA Archaeological Record* 17 (4), 8–14.
- 1045 McPherron, S. J., 2005. Artifact orientations and site formation processes from total
1046 station proveniences. *Journal of Archaeological Science* 32 (7), 1003 – 1014.
- 1047 McPherron, S. J., Dibble, H. L., Goldberg, P., 2005. Z. *Geoarchaeology* 20 (3), 243–
1048 262.
- 1049 Morton, A. G. T., 2004. Archaeological Site Formation: Understanding Lake Margin
1050 Contexts. No. 1211 in BAR International Series. Archaeopress, Oxford.
- 1051 Nickel, B., Riegel, W., Schonherr, T., Velitzelos, E., 1996. Environments of coal forma-
1052 tion in the Pleistocene lignite at Megalopolis, Peloponnese (Greece) - reconstruc-
1053 tion from palynological and petrological investigations. *N. Jb. Geol. Palaont. A.* 200,
1054 201–220.
- 1055 Ohser, J., 1983. On estimators for the reduced second moment measure of point pro-
1056 cesses. *Mathematische Operationsforschung und Statistik, series Statistics* 14, 63–
1057 71.
- 1058 Organista, E., Domínguez-Rodrigo, M., Yravedra, J., Uribe Larrea, D., Arriaza, M. C.,
1059 Ortega, M. C., Mabulla, A., Gidna, A., Baquedano, E., 2017. Biotic and abiotic pro-
1060 cesses affecting the formation of BK Level 4c (Bed II, Olduvai Gorge) and their bear-
1061 ing on hominin behavior at the site. *Palaeogeography, Palaeoclimatology, Palaeoen-*
1062 *cology*, –.
- 1063 Orton, C., 1982. Stochastic process and archaeological mechanism in spatial analysis.
1064 *Journal of Archaeological Science* 9 (1), 1 – 23.
- 1065 Panagopoulou, E., Tourloukis, V., Thompson, N., Athanassiou, A., Tsartsidou, G.,
1066 Konidaris, G., Giusti, D., Karkanas, P., Harvati, K., 2015. Marathousa 1: a new Mid-
1067 dle Pleistocene archaeological site from Greece. *Antiquity Project Gallery* 89 (343).
- 1068 Petraglia, M. D., Nash, D. T., 1987. The impact of fluvial processes on experimen-
1069 tal sites. In: Nash, D. T., Petraglia, M. D. (Eds.), *Natural formation processes and*
1070 *the archaeological record*. Vol. 352 of *International Series. British Archaeological*
1071 *Reports*, Oxford, pp. 108–130.
- 1072 Petraglia, M. D., Potts, R., 1994. Water Flow and the Formation of Early Pleistocene
1073 Artifact Sites in Olduvai Gorge, Tanzania . *Journal of Anthropological Archaeology*
1074 13 (3), 228 – 254.
- 1075 Pierson, T. C., 2005. Distinguishing between debris flows and floods from field evi-
1076 dence in small watersheds. *Usgs numbered series, U.S. Geological Survey*.

- 1077 R Core Team, 2017. R: A Language and Environment for Statistical Computing. R
1078 Foundation for Statistical Computing, Vienna, Austria.
1079 URL <https://www.R-project.org/>
- 1080 Ripley, B., 1977. Modelling spatial patterns. *Journal of the Royal Statistical Society, series B* 39, 172–212.
- 1082 Ripley, B., 1988. Statistical inference for spatial processes. Cambridge University Press.
- 1084 Ripley, B. D., 1976. The second-order analysis of stationary point processes. *Journal of Applied Probability* 13 (2), 255–266.
- 1086 Ripley, B. D., 1981. Spatial Statistics. John Wiley and Sons, New York.
- 1087 Schick, K. D., 1984. Processes of paleolithic site formation: an experimental study.
1088 Ph.D. thesis, University of California, Berkeley.
- 1089 Schick, K. D., 1986. Stone Age sites in the making: experiments in the formation
1090 and transformation of archaeological occurrences. Vol. 319 of International Series.
1091 British Archaeological Reports, Oxford.
- 1092 Schick, K. D., 1987. Modeling the formation of Early Stone Age artifact concentrations.
1093 *Journal of Human Evolution* 16, 789–807.
- 1094 Schiffer, M. B., 1972. Archaeological Context and Systemic Context. *American Antiquity* 37 (2), 156–165.
- 1096 Schiffer, M. B., 1983. Toward the identification of formation processes. *American Antiquity* 48 (4), 675–706.
- 1098 Schiffer, M. B., 1987. Formation processes of the archaeological record. University of
1099 New Mexico Press, Albuquerque.
- 1100 Shackley, M. L., 1978. The behaviour of artefacts as sedimentary particles in a fluvial environment. *Archaeometry* 20 (1), 55–61.
- 1102 Sánchez-Romero, L., Benito-Calvo, A., Pérez-González, A., Santonja, M., 12 2016.
1103 Assessment of Accumulation Processes at the Middle Pleistocene Site of Ambrona
1104 (Soria, Spain). Density and Orientation Patterns in Spatial Datasets Derived from
1105 Excavations Conducted from the 1960s to the Present. *PLOS ONE* 11 (12), 1–27.
- 1106 Texier, J.-P., 2000. A propos des processus de formation des sites préhistoriques / About
1107 prehistoric site formation processes. *Paléo* 12 (1), 379–386.
- 1108 Toots, H., 1965. Orientation and distribution of fossils as environmental indicators. In:
1109 Nineteenth Field Conference of the Wyoming Geological Association. pp. 219–292.
- 1110 Tourloukis, V., Thompson, N., Panagopoulou, E., Giusti, D., Konidaris, G., Karkanas,
1111 P., Harvati, K., this issue. Lithic and osseous artifacts from the lower palaeolithic site
1112 of marathousa 1, megalopolis, greece: preliminary results. *Quaternary International*.

- 1113 van Vugt, N., de Brujin, H., van Kolfschoten, M., Langereis, C. G., 2000. Magneto-
1114 and cyclostratigraphy and mammal-fauna's of the Pleistocene lacustrine Megalopo-
1115 lis Basin, Peloponnesos, Greece. *Geologica Ultrajectina* 189, 69–92.
- 1116 Vaquero, M., Chacón, M. G., García-Antón, M. D., de Soler, B. G., Martínez, K.,
1117 Cuartero, F., 2012. Time and space in the formation of lithic assemblages: The
1118 example of Abric Romaní Level J. *Quaternary International* 247 (0), 162 – 181.
- 1119 Villa, P., 2004. Taphonomy and stratigraphy in european prehistory. *Before Farming*
1120 2004 (1), 1–20.
- 1121 Voorhies, M., 1969. Taphonomy and population dynamics of an early pliocene ver-
1122 tebrate fauna, knox county, nebraska. *Contributions to Geology, University of*
1123 *Wyoming Special Paper* 1, 1–69.
- 1124 Walter, M. J., Trauth, M. H., 2013. A {MATLAB} based orientation analysis of
1125 acheulean handaxe accumulations in olorgesailie and kariandusi, kenya rift. *Jour-*
1126 *nal of Human Evolution* 64 (6), 569 – 581.
- 1127 Wood, R. W., Johnson, D. L., 1978. A survey of disturbance processes in archaeologi-
1128 cal site formation. In: Schiffer, M. B. (Ed.), *Advances in archaeological method and*
1129 *theory*. Vol. 1. Academic Press, Ch. 9, pp. 315–381.
- 1130 Woodcock, N., Naylor, M., 1983. Randomness testing in three-dimensional orientation
1131 data. *Journal of Structural Geology* 5 (5), 539 – 548.